

# Diffusion Model-Based Video Editing: A Survey

Wenhao Sun, Rong-Cheng Tu, Jingyi Liao, and Dacheng Tao, *Fellow, IEEE*

**Abstract**—The rapid development of diffusion models (DMs) has significantly advanced image and video applications, making “what you want is what you see” a reality. Among these, video editing has gained substantial attention and seen a swift rise in research activity, necessitating a comprehensive and systematic review of the existing literature. This paper reviews diffusion model-based video editing techniques, including theoretical foundations and practical applications. We begin by overviewing the mathematical formulation and image domain’s key methods. Subsequently, we categorize video editing approaches by the inherent connections of their core technologies, depicting evolutionary trajectory. This paper also dives into novel applications, including point-based editing and pose-guided human video editing. Additionally, we present a comprehensive comparison using our newly introduced V2VBench. Building on the progress achieved to date, the paper concludes with ongoing challenges and potential directions for future research. A project related to this paper can be found at <https://github.com/wenhao728/awesome-diffusion-v2v>.

**Index Terms**—Survey, AIGC, Diffusion model, Video editing, Video-to-video translation.

## 1 INTRODUCTION

RECENT years have witnessed remarkable development in Artificial Intelligence Generated Contents (AIGC), catalyzed by high-quality datasets and efficient computational infrastructure. Particularly in computer vision, AI’s impressive capability to generate high-dimensional perceptual data has attracted interest from researchers and exerted a profound significance on industrial products and daily life. Diffusion models [1] have emerged as a leading approach for vision generation tasks, including Text-to-Image (T2I) generation [2], [3], [4], [5], [6], [7], [8] and Image-to-Image (I2I) translation [9], [10], [11], [12], [13], [14], [15], [16]. These methods can generate high-quality semantically accurate images from text descriptions or modify input images based on specified conditions.

Considering that videos are primarily composed of continuous image sequences, there is a natural inclination to extend the success of diffusion models from 2D image generation to 3D video generation and editing, which has sparked considerable research interest. However, extending these architectures to videos introduces challenges, mainly in adapting designs for static images to handle videos’ dynamic and temporal aspects. The scarcity of high-quality video datasets adds further technical difficulties. Researchers must tackle effective video dataset curation or consider alternative surrogate tasks and other solutions.

Despite these challenges, recent advancements have been witnessed in diffusion model-based video generative methods [17], [18], [19], [20], [21], [22]. Among these methods, the most influential areas are generating videos from text inputs and editing existing videos generatively. Furthermore, editing existing videos does not require prohibitively expensive video pre-training and allows fine-grained control of the source video, leading to diverse applications, as illustrated in Figure 1.

As the field of diffusion-based video editing continues to expand, there is a growing need for a detailed survey that helps readers stay informed about recent advancements. However, existing surveys on diffusion models primarily focus on other aspects or tasks, such as the theoretical formulation of diffusion processes [23], [24], [25], [26], image generation [27], [28], image editing [29], and 3D object generation [30], [31]. While some surveys mentioned video editing [30], [32], they only provide a brief overview, missing influential methods, detailed narration, and the underlying linkages within these emerging approaches.

This paper provides a thorough review of diffusion model-based video editing technologies. It covers a broad spectrum of editing tasks, methodologies, and evaluations, offering valuable insights. This survey not only deepens the understanding of the current landscape but also outlines potential developments and applications, highlighting directions for future research.

This paper is structured as follows: In Section 2, we review the preliminaries, including the mathematical formulation of diffusion models, related approaches in 2D image generation, and video generation methods. Subsequently, Section 3 categorizes diffusion model-based video editing approaches into five primary classes based on their underlying technologies. Section 4 introduces a new benchmarking, V2VBench, encompassing four text-guided video editing tasks, along with a detailed evaluation and analysis. Finally, in Section 5, we summarize the open challenges and outline emerging research trends.

## 2 BACKGROUND

This section presents an overview of the essential preliminaries for diffusion model-based video editing methods. We start with the mathematical framework of diffusion models (Section 2.1), followed by an exploration of image generation and editing techniques (Section 2.2). We then shift to the video domain, providing an overview of diffusion models for video generation and consolidating motion

- Wenhao Sun, Rong-Cheng Tu, Jingyi Liao, and Dacheng Tao are with the College of Computing and Data Science, Nanyang Technological University.  
E-mail: {wenhao006, rongcheng.tu, jingyi012, dacheng.tao}@ntu.edu.sg.
- Dacheng Tao is the corresponding author.

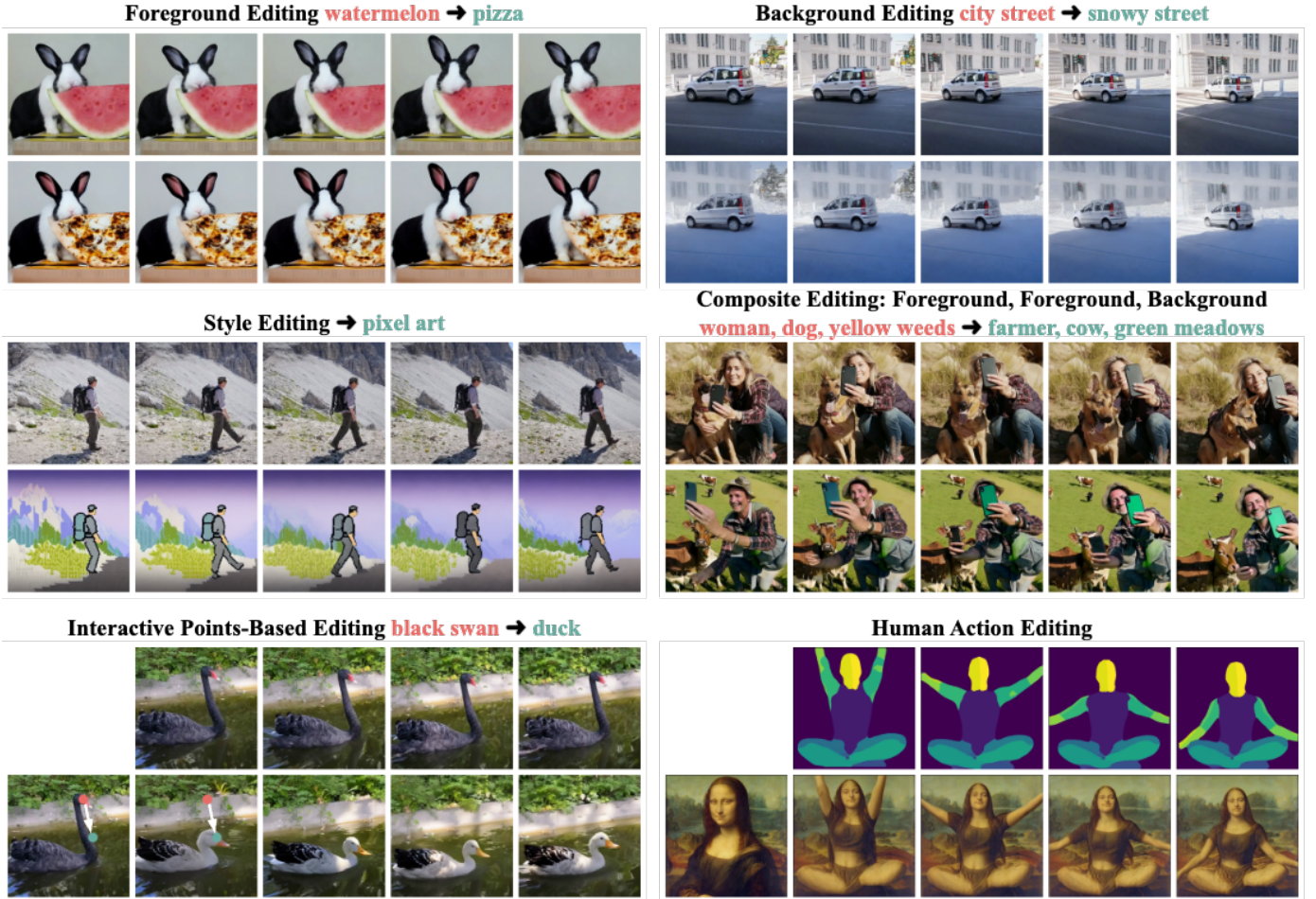


Fig. 1. This survey focuses on video editing and video-to-video translation tasks. Results depicted here are sourced from [33], [34], [35], [36], [37], [38] and will be discussed in Section 3.

representation in Section 2.3. We focus on the discrete formulation of the diffusion process [39] and highlight the core contributions of representative works to maintain focus and conciseness.

## 2.1 Mathematical Framework

Diffusion models [1] fall within the family of latent probabilistic models, alongside variational autoencoders (VAEs) [40], [41], normalization flows [42], *etc.* They are distinguished by possessing an analytical form of the latent distribution. Specifically, consider a sample  $\mathbf{z}_0$  randomly drawn from the training dataset, with each sample i.i.d. following an underlying distribution  $q(\mathbf{z}_0)$ . The posterior distribution is defined by a Markov chain  $q(\mathbf{z}_{1:T}|\mathbf{z}_0) = \prod_{t=1}^T q(\mathbf{z}_t|\mathbf{z}_{t-1})$ , known as the forward diffusion process, which gradually adds Gaussian noise into the data:

$$q(\mathbf{z}_t|\mathbf{z}_{t-1}) := \mathcal{N}(s_t\mathbf{z}_{t-1}, \sigma_t^2\mathbf{I}). \quad (1)$$

The Markov chain hyperparameters  $s_t = \sqrt{\alpha_t/\alpha_{t-1}}$  and  $\sigma_t = \sqrt{1 - \alpha_t/\alpha_{t-1}}$  can be assigned to facilitate the variance preservation formulation [39], [43]. Here, the  $\{\alpha_t\}_{t=0}^T$  denote a predefined set of hyperparameters that adhere to  $0 < \alpha_T < \dots < \alpha_0 = 1$ .

The underlying data distribution  $q(\mathbf{z}_0)$ , is estimated with the form  $p_\theta(\mathbf{z}_0) = \int p_\theta(\mathbf{z}_{0:T})d\mathbf{z}_{1:T}$ . The joint distribution

$p_\theta(\mathbf{z}_{0:T})$ , known as the reverse diffusion process, is commonly assumed to follow a Markov chain [1], [39] with learnable transition distribution:

$$p_\theta(\mathbf{z}_{t-1}|\mathbf{z}_t) := \mathcal{N}(\mu_\theta(\mathbf{z}_t, t), \Sigma_\theta(\mathbf{z}_t, t)), \quad (2)$$

where  $\theta$  represents the trainable parameters.

### 2.1.1 Diffusion Model Properties

**Gaussian Marginal Distribution.** The marginal distribution of the forward diffusion process follows Gaussian [1]:

$$q(\mathbf{z}_t|\mathbf{z}_0) := \mathcal{N}(\sqrt{\alpha_t}\mathbf{z}_0, (1 - \alpha_t)\mathbf{I}). \quad (3)$$

This implies that the forward diffusion process can be achieved by directly interpolating between noise  $\epsilon_t \sim \mathcal{N}(\mathbf{0}, \mathbf{I})$  and the initial latent (clean sample)  $\mathbf{z}_0$  without considering intermediate latents. When  $\alpha_T$  is sufficiently closed to 0,  $q(\mathbf{z}_T|\mathbf{z}_0)$  converges towards a standard Gaussian distribution  $\mathcal{N}(\mathbf{0}, \mathbf{I})$  for arbitrary  $\mathbf{z}_0$ .

**Score.** The score function is the gradient of the log-density with respect to the data vector [44]. Assuming a Gaussian distribution, the score takes the following form [43]:

$$\nabla_{\mathbf{z}_t} \log q(\mathbf{z}_t|\mathbf{z}_0) = -\frac{\mathbf{z}_t - \sqrt{\alpha_t}\mathbf{z}_0}{1 - \alpha_t} = -\frac{\epsilon_t}{\sqrt{1 - \alpha_t}}, \quad (4)$$

where  $\epsilon_t \sim \mathcal{N}(\mathbf{0}, \mathbf{I})$  is a standard Gaussian random variable.

### 2.1.2 Diffusion Model Optimization

The diffusion models can be trained by optimizing the Evidence Lower Bound (ELBO) [39]:

$$\text{ELBO} = \mathbb{E}_q \left[ \log \frac{p_\theta(\mathbf{z}_{0:T})}{q(\mathbf{z}_{1:T}|\mathbf{z}_0)} \right]. \quad (5)$$

After parameterization, the training is represented as an  $\epsilon$ -prediction task [39], [45]:

$$\mathcal{L} = \mathbb{E}_{t, \mathbf{z}_t, \epsilon_t \sim \mathcal{N}(\mathbf{0}, \mathbf{I})} [\lambda(t) \|\epsilon_t - \epsilon_\theta(\mathbf{z}_t, t)\|_2^2], \quad (6)$$

where  $\lambda(t) > 0$  serves as a weighting term dependent on  $t$ . Ho *et al.* [39] discovered that setting  $\lambda(t) \equiv 1$  in Equation (6) enhances network learning by emphasizing the more challenging instances with larger  $t$ . Consequently, they simplified Equation (6) to:

$$\mathcal{L}_{\text{simple}} = \mathbb{E}_{t, \mathbf{z}_t, \epsilon_t} [\|\epsilon_t - \epsilon_\theta(\mathbf{z}_t, t)\|_2^2]. \quad (7)$$

### 2.1.3 Reverse Diffusion Sampling

The formulation of reverse diffusion sampling is:

$$\mathbf{z}_{t-1} = \sqrt{\alpha_{t-1}} \mathbf{z}_{t \rightarrow 0} + \sqrt{1 - \alpha_{t-1} - \sigma_t^2} \epsilon_\theta(\mathbf{z}_t, t) + \sigma_t \nu_t, \quad (8)$$

$$\text{where } \mathbf{z}_{t \rightarrow 0} = \frac{1}{\sqrt{\alpha_t}} (\mathbf{z}_t - \sqrt{1 - \alpha_t} \epsilon_\theta(\mathbf{z}_t, t)), \quad (9)$$

$$\text{and } \sigma_t = \sqrt{(1 - \alpha_{t-1}) / (1 - \alpha_t)} \cdot \sqrt{1 - \alpha_t / \alpha_{t-1}}.$$

Here  $\nu_t \sim \mathcal{N}(\mathbf{0}, \mathbf{I})$  denotes standard Gaussian random variable that is independent of  $\mathbf{z}_t$ .

One practical limitation of Equation (8) is its requirement for  $T$  denoising interactions, which is typically set to a large value (*e.g.*  $T = 1000$ ) to conform to the Gaussian assumption. To accelerate the reverse sampling process, DDIM [46] proposes representing the diffusion process through a non-Markov chain, while retaining the identical objective function as in Equation (6). This non-Markov process allows for the flexibility to sample fewer steps (*e.g.*  $T = 50$ ) without altering the pre-trained weights. DDIM sampling follows a similar sampling formulation as Equation (8), but it is a deterministic process with  $\sigma_t = 0$ :

$$\mathbf{z}_{t-1} = \sqrt{\alpha_{t-1}} \mathbf{z}_{t \rightarrow 0} + \sqrt{1 - \alpha_{t-1}} \epsilon_\theta(\mathbf{z}_t, t). \quad (10)$$

## 2.2 Image Diffusion Models

This section primarily discusses the image diffusion methods. In practical implementations, the diffusion process often occurs in a semantically equivalent space rather than the original data space (*e.g.* the VAE latent space versus the pixel space of an image dataset). To avoid ambiguity, we denote the original image samples as  $\mathbf{x}_0$  and the noise-free samples in the diffusion process as  $\mathbf{z}_0$  throughout the paper.

Early image diffusion models [39], [45], [47], [48], [49], [50] directly generate images at the desired resolution, *i.e.*  $\mathbf{z}_0 = \mathbf{x}_0$ . As a result, early image diffusion models typically produced images at low resolutions. Generating high-resolution images is prohibitively expensive.

To address the high-resolution challenge, Cascaded Diffusion Models (CDMs) [3], [4], [51] propose initiating generation at lower resolutions and then upsampling by super-resolution diffusion models. In this scenario, the samples

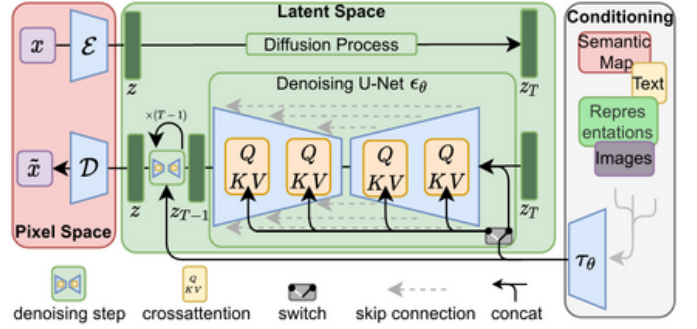


Fig. 2. The architecture of LDM [5]. It consists of an encoder  $\mathcal{E}$ , a decoder  $\mathcal{D}$ , and a UNet noise predictor  $\epsilon_\theta$  with cross-attention blocks to incorporate conditioning from domain encoders  $\tau_\theta$ . Figure adapted from LDM [5].

for diffusion models training are derived from the down-sampled pixel-level images  $\mathbf{z}_0 = \text{DownSample}(\mathbf{x}_0)$ .

More recently, Latent Diffusion Models (LDMs) [5], [52] can generate high-resolution images at affordable computational cost by operating within the latent space of a pre-trained VAE [40], [41], [53]. This approach capitalizes on the observation: VAEs excel at perceptual compression by effectively removing and reconstructing high-frequency details; diffusion models excel at capturing the semantic and conceptual composition of the data [5]. Specifically, people train diffusion models in the VAEs' lower-dimensional latent space:  $\mathbf{z}_0 = \mathcal{E}(\mathbf{x}_0)$ , where  $\mathcal{E}$  represents a VAE encoder. During inference, the diffusion model outputs are mapped back to the pixel space  $\mathbf{x}_0 = \mathcal{D}(\mathbf{z}_0)$  by the VAE decoder  $\mathcal{D}$ . The architecture proposed by Rombach *et al.* [5] is illustrated in Figure 2.

### 2.2.1 Conditioning and Guidance

Conditional generation has emerged as one of the most important tasks for image generation. Common conditions include class labels [39], [43], [47], [48], text [2], [3], [4], [5], [6], [51], [52], depth maps [54], [55], *etc.* Then, we survey the architecture design to incorporate conditions and the guidance mechanisms. To avoid confusion, we explicitly declare the conditional input in the noise predictor:  $\epsilon_\theta(\mathbf{z}_t, t, y)$  represents the noise prediction with condition  $y$ ;  $\epsilon_\theta(\mathbf{z}_t, t, \emptyset)$  represents the unconditional prediction.

**Spatial-Aligned Conditions.** Many condition variants are spatial aligned with the target image, including depth maps, segmentation maps, and spatial layouts. One straightforward solution is to concatenate these conditions with the noisy latent state  $\mathbf{z}_t$  and pass them as input to the noise predictor  $\epsilon_\theta$ . Various I2I translation tasks, such as inpainting and colorization, can be treated as conditional image generation and addressed using this approach [5], [10].

Researchers later propose to use the adapter to efficiently handle various spatial alignment conditions without modifying the pre-trained diffusion model parameters. Two iconic works, T2I-Adapter [55] and ControlNet [54], offer flexible solutions by adding hyper-networks to the pre-trained model. Specifically, they propose duplicating the encoder blocks of the pre-trained UNet noise predictor and reintegrating their outputs. T2I-Adapter adds the multi-scale hyper-network outputs to the UNet encoder blocks.

Conversely, the ControlNet outputs are connected to the decoder blocks by zero convolutions to ensure stability in the initial training steps. Since the parameters remain unchanged, a single pre-trained network can be integrated with multiple adapters for various tasks.

**Adaptive Normalization.** Another approach to incorporate conditions into diffusion models is applying the feature-wise transformation [56]:  $\text{AdaNorm}(\mathbf{h}) = s_y \text{Norm}(\mathbf{h}) + b_y$ , where  $s_y \in \mathbb{R}$  and  $b_y \in \mathbb{R}$  are derived from condition  $y$ . Group Normalization [57] and Instance Normalization [58], [59] are common options for hidden feature normalization. This approach has empirically demonstrated promising results for the time steps and class labels [47], [48].

**Conditioning by Cross Attention.** Many advanced diffusion methods [2], [4], [5] incorporate transformer blocks [60] in their networks and use cross-attention to integrate conditions. A domain-specific encoder  $\tau_\theta(\cdot)$  first encodes the condition  $y$ :  $\tau_\theta(y) \in \mathbb{R}^{d_r \times L}$ . Then, the cross-attention layers  $\text{Attn}(\mathbf{Q}, \mathbf{K}, \mathbf{V}) = \text{softmax}(\mathbf{Q}^T \cdot \mathbf{K} / \sqrt{d}) \cdot \mathbf{V}^T$  can be formulated as:

$$\mathbf{Q} = \mathbf{W}_Q \cdot \mathbf{h}, \mathbf{K} = \mathbf{W}_K \cdot \tau_\theta(y), \mathbf{V} = \mathbf{W}_V \cdot \tau_\theta(y), \quad (11)$$

where  $\mathbf{h} \in \mathbb{R}^{d \times N}$  denotes the flattened hidden feature of the noise predictor  $\epsilon_\theta(\cdot)$ .  $\mathbf{W}_Q \in \mathbb{R}^{d \times d}$ ,  $\mathbf{W}_K \in \mathbb{R}^{d \times d_r}$ , and  $\mathbf{W}_V \in \mathbb{R}^{d \times d_r}$  denote learnable projection matrices. Text descriptions and reference images are common cross-attention conditions.

**Classifier Guidance.** In addition to the model inputs, Sohl-Dickstein *et al.* [1] and Song *et al.* [43] propose using pre-trained classifier  $\mathcal{C}(\cdot)$ , which predicts the class probability of the intermediate diffusion latents, to guide the generation process of diffusion models. They formulate the estimated score function as follows:

$$\begin{aligned} \nabla_{\mathbf{z}_t} \log p_\theta(\mathbf{z}_t, y) &= \nabla_{\mathbf{z}_t} \log p_\theta(\mathbf{z}_t) + \nabla_{\mathbf{z}_t} \log \mathcal{C}(y|\mathbf{z}_t) \quad (12) \\ &= -\frac{1}{\sqrt{1-\alpha_t}} (\epsilon_\theta(\mathbf{z}_t, t, \emptyset) - \sqrt{1-\alpha_t} \nabla_{\mathbf{z}_t} \log \mathcal{C}(y|\mathbf{z}_t)), \end{aligned}$$

Thus, a new classifier-guided noise predictor takes the following form:

$$\epsilon_\theta(\mathbf{z}_t, t, y) \leftarrow \epsilon_\theta(\mathbf{z}_t, t, \emptyset) - w\sqrt{1-\alpha_t} \nabla_{\mathbf{z}_t} \log \mathcal{C}(y|\mathbf{z}_t), \quad (13)$$

where a scale  $w$  is added to control the guidance strength.

**Classifier-Free Guidance.** Ho & Salimans [49] propose guiding the diffusion generation process without pre-trained classifiers. They apply Bayes' theorem to formulate the classifier gradient  $\nabla_{\mathbf{z}_t} \log \mathcal{C}(y|\mathbf{z}_t)$  using the conditional score function and unconditional score function:

$$\begin{aligned} \nabla_{\mathbf{z}_t} \log \mathcal{C}(y|\mathbf{z}_t) &= \nabla_{\mathbf{z}_t} \log p_\theta(\mathbf{z}_t|y) - \nabla_{\mathbf{z}_t} \log p_\theta(\mathbf{z}_t) \quad (14) \\ &= -\frac{1}{\sqrt{1-\alpha_t}} (\epsilon_\theta(\mathbf{z}_t, t, y) - \epsilon_\theta(\mathbf{z}_t, t, \emptyset)), \end{aligned}$$

which is substituted into Equation (13), resulting in a new classifier-free predictor:

$$\begin{aligned} \epsilon_\theta(\mathbf{z}_t, t, y) &\leftarrow \epsilon_\theta(\mathbf{z}_t, t, \emptyset) - w\sqrt{1-\alpha_t} \nabla_{\mathbf{z}_t} \log \mathcal{C}(y|\mathbf{z}_t) \quad (15) \\ &= \epsilon_\theta(\mathbf{z}_t, t, \emptyset) + w(\epsilon_\theta(\mathbf{z}_t, t, y) - \epsilon_\theta(\mathbf{z}_t, t, \emptyset)). \end{aligned}$$

During training, the condition  $y$  is randomly set to empty  $\emptyset$ , allowing a single predictor to handle both conditional and unconditional inputs.

This classifier-free guidance can naturally extend to multiple conditions with a hierarchical structure. Here, we illustrate the scenario with two conditions; additional scenarios can be similarly extended:

$$\begin{aligned} \epsilon_\theta(\mathbf{z}_t, t, y_1, y_2) &\leftarrow \epsilon_\theta(\mathbf{z}_t, t, \emptyset, \emptyset) \quad (16) \\ &+ w_1 (\epsilon_\theta(\mathbf{z}_t, t, y_1, \emptyset) - \epsilon_\theta(\mathbf{z}_t, t, \emptyset, \emptyset)) \\ &+ w_2 (\epsilon_\theta(\mathbf{z}_t, t, y_1, y_2) - \epsilon_\theta(\mathbf{z}_t, t, y_1, \emptyset)). \end{aligned}$$

### 2.2.2 Editing and Customization

Closely related to conditional generation, image editing concentrates on generating images while maintaining specific attributes of a source image, such as the identity of subjects, background, spatial layout, *etc.* Here, we discuss image editing techniques that extend beyond traditional conditioning mechanisms.

**Latent State Initialization.** Image diffusion models typically initialize the latent states with Gaussian noise [1], [39], [45], [50]. To preserve low-frequency structures while editing high-frequency details, SDEdit [61] perturbs the source image through the forward diffusion process, as indicated in Equation (3), then generates the target image from the partially perturbed latent state. Many feasible images can correspond to the same initial latent state, and conditions and guidance techniques from Section 2.2.1 are employed to direct the editing process [9].

Instead of perturbing the source image with randomness, the latent state can be initialized using the reverse diffusion process [46]. Specifically, the sampling formula in Equation (10) is algebraically manipulated as follows:

$$\mathbf{z}_t = \sqrt{\frac{\alpha_t}{\alpha_{t-1}}} \mathbf{z}_{t-1} + \left( \sqrt{1-\alpha_t} - \sqrt{\frac{\alpha_t}{\alpha_{t-1}} - \alpha_t} \right) \epsilon_\theta(\mathbf{z}_t, t, y). \quad (17)$$

$\mathbf{z}_t$  appears on both sides of Equation (17). Assuming Gaussian transitions and small step sizes,  $\mathbf{z}_t$  can be approximated by replacing  $\epsilon_\theta(\mathbf{z}_t, t)$  on the right-hand side of Equation (17) with  $\epsilon_\theta(\mathbf{z}_{t-1}, t)$ , resulting in the following approximation:

$$\mathbf{z}_t \approx \sqrt{\frac{\alpha_t}{\alpha_{t-1}}} \mathbf{z}_{t-1} + \left( \sqrt{1-\alpha_t} - \sqrt{\frac{\alpha_t}{\alpha_{t-1}} - \alpha_t} \right) \epsilon_\theta(\mathbf{z}_{t-1}, t, y). \quad (18)$$

The source image is inverted into latent states by iteratively applying Equation (18). Note that the inversion process can be made unconditional by setting  $y = \emptyset$ . Then, reverse diffusion sampling on the inverted latent states leads to deterministic reconstruction with negligible error when using the inversion condition  $y$ , and enables editing when using the target condition  $\hat{y}$ .

When incorporating classifier-free guidance [49], the  $w > 1$  guidance scale amplifies the approximation error, which further accumulates throughout the diffusion process. Null-text inversion [62] addresses this issue by regressing the 'null text' embedding at each denoising step. For each timestep  $t = T, \dots, 1$ , the null-text embeddings can be iteratively optimized using the following formula:

$$\hat{\emptyset}_t = \arg \min_{\emptyset_t} \|\mathbf{z}_{t-1}^u - \mathbf{z}_{t-1}(\mathbf{z}_t, t, y, \emptyset_t)\|_2^2, \quad (19)$$

where  $\mathbf{z}_{t-1}^u$  represents the unconditional inversion. And  $\mathbf{z}_{t-1}(\mathbf{z}_t, t, y, \emptyset_t)$  is the latent obtained from the inversion

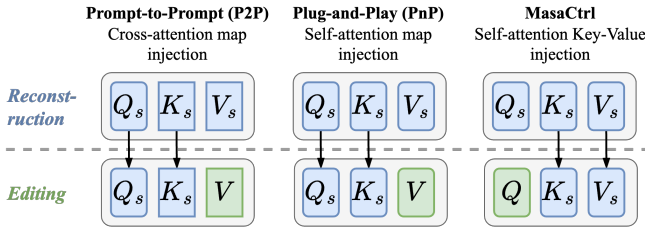


Fig. 3. Feature injection methods for image editing. P2P [13] injects cross-attention maps from the reconstruction branch into the editing branch. PnP [14] injects self-attention maps. While MasaCtrl [15] injects self-attention query and key features.

process described in Equation (18), with its noise predicted using classifier-free guidance as described in Equation (15). **Attention Feature Injection.** The network attention maps and hidden features possess abundant semantic and spatial information [63]. Several methods focus on denoising with dual branches in parallel and selectively inject attention maps and hidden features from one branch to another, ensuring consistency and editability simultaneously. Specifically, this paradigm employs a reconstruction branch for source images and an editing branch for target images as illustrated in Figure 3.

Prompt-to-Prompt (P2P) [13] emphasizes the efficacy of text prompts in T2I diffusion models. It injects the cross-attention map of unchanged tokens from the reconstruction branch into the editing branch, thereby preserving the unaltered area of source images. Plug-and-Play (PnP) [14] and MasaCtrl [15] emphasize the importance of self-attention layers as structural descriptors. PnP injects self-attention query, key, and each block’s output from the reconstruction branch to the editing branch, ensuring the preservation of semantic layout. On the other hand, MasaCtrl maintains the query features unchanged while transferring key and value features. It uses the injection masks by thresholding the cross-attention maps of edited words [64], [65] to address foreground-background confusion. Feature injection methods can start by inverting the source image through latent inversion, as shown in Equations (18) and (19). Subsequently, the inverted latent states are used for both branches. **Text Inversion.** Text conditions are pivotal in denoising when noisy images offer limited information during earlier reverse diffusion steps [7]. Textural Inversion [66] optimizes a token embedding, serving as an identifier to maintain the protagonist’s identity. DreamBooth [67] employs an identifier alongside the subject’s class name, capturing semantic information and finer details by fine-tuning the base and super-resolution components of Imagen [4] using 3-5 images. Continuing in this direction, subsequent studies [68], [69], [70], [71], [72], [73] have achieved precise attribute control and interesting applications such as conceptual interpolation.

Among these image editing methods, latent state initialization methods are proficient in large features and pose changes [74]. Feature injection methods excel in stylization, background, and object replacements, while text inversion methods are more suitable for object customization and personalization. Many orthogonal methods can be collab-

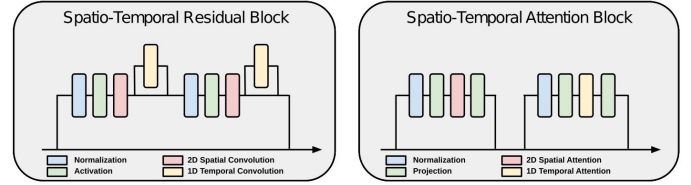


Fig. 4. The temporal extension from image to video models involves incorporating 1D temporal convolutions after each 2D spatial convolution (left). Additionally, each 2D spatial attention block is followed by a 1D temporal attention block (right). Figure adapted from Gen-1 [94].

oratively employed to address diverse editing tasks.

### 2.2.3 Efficient Adaptions

Low-Rank Adaptation (LoRA) [75] is a widely recognized matrix reparameterization technique. For a pre-trained parameter matrix  $\mathbf{W} \in \mathbb{R}^{d \times k}$ , LoRA introduces two low-rank factorized matrices  $\mathbf{A} \in \mathbb{R}^{d \times r}$ ,  $\mathbf{B} \in \mathbb{R}^{r \times k}$ , and  $r \ll \min(d, k)$  to represent its training updates  $\Delta \mathbf{W} = \mathbf{A} \cdot \mathbf{B} \in \mathbb{R}^{d \times k}$ . Only the factorized matrices,  $\mathbf{A}$  and  $\mathbf{B}$ , are trainable:  $\mathbf{W} \leftarrow \mathbf{W} + \mathbf{A} \cdot \mathbf{B}$ . LoRA can be intuitively applied to many network layers, including attention and MLP. It offers significant advantages in lower memory consumption and faster convergence.

Token Merging (ToMe) [76], [77] is an efficient adaptation to increase the throughput of Vision Transformer (ViT) [78] architecture. ToMe reduces the number of tokens processed by merging similar tokens before attention layers. This merging operation uses bipartite soft matching, where tokens are alternatively partitioned into two sets, and the top  $r$  most similar tokens between these sets are merged. ToMe later extends to dense prediction tasks, such as image generation. For StableDiffusion [5], ToMe happens before self-attention layers, with outputs unmerged to maintain the token count. This approach doubles the image generation speed and reduces memory consumption by up to  $5.6 \times$  with negligible quality degradation.

## 2.3 Video Generation and Motion Representation

Video generation aims to create videos from scratch, sharing many underlying technologies with video editing. Recent advancements in diffusion models [17], [18], [19], [20], [21], [79], [80], [81], [82], [83], [84] have accelerated video generation progress, surpassing previous GANs [85], [86], [87], [88], [89], [90], [91]. We next review key technologies in video generation (Section 2.3.1). Following that, Section 2.3.2 introduces optical flow [92], [93], a motion representation technique widely used in various video-related tasks.

### 2.3.1 Diffusion Models for Video Generation

Pre-trained image diffusion models are well-known for their 2D modeling capabilities. Since video frames are sequential images, extending these image priors to video tasks is a logical progression. The seminal work, Video Diffusion Models (VDM) [17], adopts a factorized 3D architecture that separately processes the 2D spatial and 1D temporal dimensions. Figure 4 illustrates two variants of 3D blocks: 1D temporal convolutions are incorporated through residual connections after each 2D spatial convolution; attention

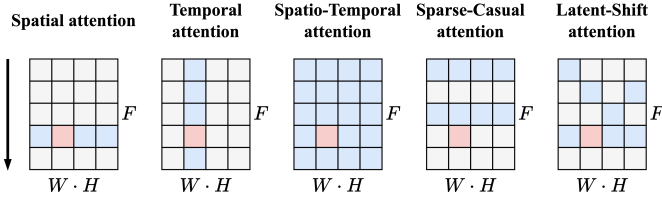


Fig. 5. Self-attention variations. The query tokens are in red, and the key and value tokens are in blue.  $W$ ,  $H$ , and  $F$  denote the input video’s width, height, and frame numbers.

blocks apply a similar architecture. This design facilitates cross-frame interaction at a relatively low cost, mitigating the computational burden imposed by the curse of dimensions. Figure 5 also illustrates the distinction between spatial attention, temporal attention, and full 3D spatial-temporal attention, with the two spatial dimensions flattened for clarity. From the training data perspective, VDM facilitates image-video joint learning to tackle the challenges posed by video datasets, which typically exhibit lower quality and quantity than image datasets.

Subsequent studies extend the success of CDM and LDM in the Text-to-Video (T2V) domain on larger data and model scales. Models such as ModelScope [80], Show-1 [81], VideoCrafter [82], [95], and LaVie [83] serve as large-scale open-source baselines, leveraging pre-trained T2I diffusions for efficient training. GenTron [84] and LATTE [21] utilize a pure transformer backbone in video diffusion models. Additionally, Latent-Shift [96] explores the latent-shift attention (as shown in Figure 5) in video generation tasks as an alternative implementation for spatiotemporal modeling. AnimateDiff [20] showcases the orthogonal learning of appearance and motion. It freezes the original spatial weights while learning adaptable temporal layers on video datasets. Once the temporal layers are trained, they can serve as plugins, enabling various customized image diffusion models from the community to gain animation capabilities without retraining on video data.

In addition to T2V, many works primarily focus on Image-to-Video (I2V) [22], [97], [98], [99], [100], [101] and video completion [102], [103] tasks, where a single frame or short video clip is provided, intending to generate longer videos. Other conditional modalities include audio [104], [105], [106], structure [107], [108], and even MRI signals [109]. Multi-modal guided video generation [110], [111], [112] is also actively pursued.

### 2.3.2 Motion Representation

Dense optical flow [92], [93] is an iconic representation of video motion information, which depicts each pixel’s horizontal and vertical offset. It finds extensive utility in point tracking [93], [113], video compression [114], evaluation metrics [115], [116], and more. Many optical flow estimation models [117], [118], trained and validated using simulated ground-truth datasets [119], [120], [121], [122], exhibit robust generalization to realistic scenarios.

Let us denote the optical flow from the source frame  $\mathbf{x}^{f_1} \in \mathbb{R}^{3 \times W \times H}$  to the target frame  $\mathbf{x}^{f_2} \in \mathbb{R}^{3 \times W \times H}$  as  $\mathcal{F}^{f_1 \rightarrow f_2} \in \mathbb{R}^{2 \times W \times H}$ . Certain regions may lack accurate correspondence, often indicated by occlusion masks

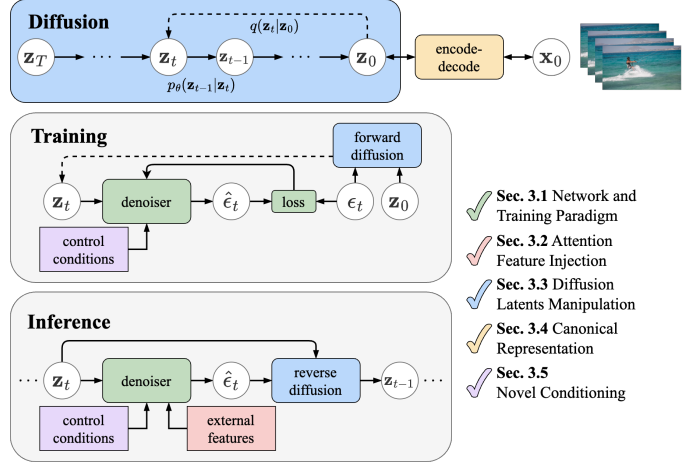


Fig. 6. Overview of diffusion-based video editing components.

$\mathcal{O}^{f_1 \rightarrow f_2} \in \{0, 1\}^{W \times H}$ . The operation of estimating the target frame  $\mathbf{x}^{f_2}$  from an optical flow  $\mathcal{F}^{f_1 \rightarrow f_2}$  and a source frame  $\mathbf{x}^{f_1}$  is known as warping  $\mathcal{F}^{f_1 \rightarrow f_2}(\mathbf{x}^{f_1})$ .

## 3 DIFFUSION MODEL-BASED VIDEO EDITING

Building on the generation concept, editing tasks focus on altering existing content rather than generating new material from scratch. Video editing tasks, also known as Video-to-Video (V2V) translation, use the source video  $\mathbf{x}_0^s$  and the target prompt  $y$  serve as inputs to generate the desired changes in the resulting video  $\mathbf{x}_0$ .

Figure 6 depicts the components in a general video editing diffusion model. This section starts with a detailed review of the network and training paradigm modifications (Section 3.1), followed by attention feature injection technologies for effective video editing (Section 3.2), diffusion latents manipulation (Section 3.3), and canonical video representation (Section 3.4). Finally, we introduce approaches with novel control conditions (Section 3.5). Some methods employ multiple technologies and overlap with various sections; we introduce them based on their primary concentration. Figure 7 provides an overview of all methods covered for quick reference.

### 3.1 Network and Training Paradigm

Applying image editing methods to videos on a frame-by-frame basis introduces temporal inconsistency and quality degradation issues. This section explores various network and training paradigm modifications, including network layer design, structure conditioning, and training modification. These methods collectively reveal the evolving effectiveness and complexity of video editing tasks.

#### 3.1.1 Temporal Adaptation

Tune-A-Video [163] pioneers the concept of one-shot tuning in video editing. It transforms the spatial self-attention layers of a T2I StableDiffusion into the sparse-casual attention layers. As illustrated in Figure 5, this mechanism employs the key-value features drawn from both the first frame  $\mathbf{h}^1$  and the preceding frame  $\mathbf{h}^{f-1}$  to update the current frame

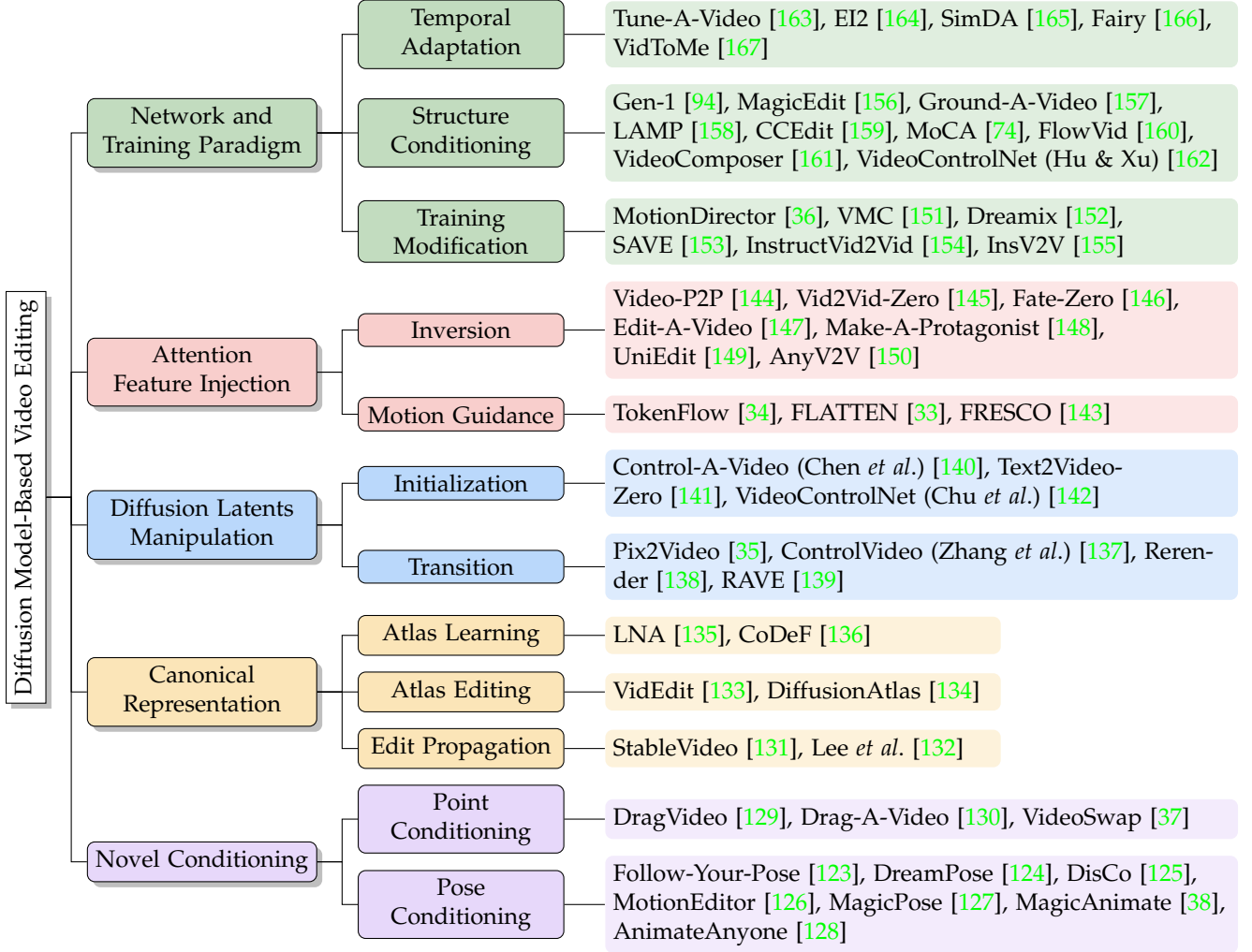


Fig. 7. Taxonomy of diffusion-based video editing methods.

features. The query, key, and value features for frame  $f$  are defined as follows:

$$\begin{aligned} \mathbf{Q}^f &= \mathbf{W}_Q \cdot \mathbf{h}^f, \\ \mathbf{K}^f &= \mathbf{W}_K \cdot [\mathbf{h}^1, \mathbf{h}^{f-1}], \\ \mathbf{V}^f &= \mathbf{W}_V \cdot [\mathbf{h}^1, \mathbf{h}^{f-1}], \end{aligned} \quad (20)$$

where  $[\cdot]$  denotes concatenation along the sequence dimension, and  $\mathbf{W}_Q \in \mathbb{R}^{d \times d}$ ,  $\mathbf{W}_K \in \mathbb{R}^{d \times d}$ , and  $\mathbf{W}_V \in \mathbb{R}^{d \times d}$  represent the projection matrices. To effectively capture the structure and motion of the source video, Tune-A-Video fine-tunes the query projection matrices of sparse-causal attention, query projection matrices of cross-attention layers, and the newly introduced temporal attention layers. During the inference phase, this method uses DDIM-inverted latents [46] to initiate the generation, thereby ensuring the preservation of characteristics from the source video.

EI2 [164] analyzes the covariate shifting caused by the temporal attention layers in Tune-A-Video [163]. It identifies a deficiency of the Layer Normalization to adequately center the hidden features  $\mathbf{h} \in \mathbb{R}^{d \times F \times W \times H}$  along the temporal dimension. As a solution, it proposes an Instance Centering

(IC) layer as the replacement:

$$\text{IC}(\mathbf{h}) = \mathbf{h} - \frac{1}{F \cdot W \cdot H} \sum_{f=1}^F \sum_{i=1}^W \sum_{j=1}^H \mathbf{h}_{[i,j]}^f. \quad (21)$$

Moreover, Spectral Normalization [168] is incorporated to mitigate covariate shifts. Furthermore, EI2 enhances its approach by concatenating downsampled inter-frame features as self-attention key and value features, facilitating efficient spatio-temporal interaction.

**Parameter-Efficient Approaches.** While effective, methods like Tune-A-Video entail high fine-tuning costs. SimDA [165] aims to extend T2I StableDiffusion to T2V by parameter efficient fine-tuning. It utilizes an adapter comprising two learnable fully connected (FC) layers:  $\mathbf{W}_{\text{down}} \in \mathbb{R}^{d' \times d}$  and  $\mathbf{W}_{\text{up}} \in \mathbb{R}^{d \times d'}$ , along with an intermediate layer  $\mathcal{L}(\cdot)$ :

$$\text{Adapter}(\mathbf{h}) = \mathbf{h} + \mathbf{W}_{\text{up}} \cdot \mathcal{L}(\mathbf{W}_{\text{down}} \cdot \mathbf{h}). \quad (22)$$

The first FC layer maps the input  $\mathbf{h} \in \mathbb{R}^{d \times F \times W \times H}$  to a lower-dimension vector space ( $d' < d$ ), while the second layer maps it back. SimDA incorporates spatial adapters to learn appearance transferability and temporal adapters to model temporal information. The intermediate layers utilize GELU activations [169] and depth-wise 3D convolutions

for spatial and temporal adapters, respectively. Additionally, SimDA implements the temporally latent-shifted self-attention [96], [170], shown in Figure 5, to enhance temporal consistency. This approach thus benefits from both computational efficiency and temporal perception.

Fairy [166] is designed for parallelized frames sampling. First, some keyframes are sampled in an interleaved manner. These keyframes are edited in a single forward pass, utilizing a 3D spatio-temporal self-attention extended from a T2I diffusion model. Fairy independently processes the remaining frames using an instruction-based I2I diffusion model [16], facilitating parallel processing. The self-attention layers of the I2I model are adjusted to integrate additional key and value features from the keyframes, providing supplementary guidance to ensure temporal consistency. The I2I model is fine-tuned using affine augmentation, applied identically and randomly to both source and target images, ensuring robustness in movements.

VidToMe [167] leverages temporal redundancy in videos to enhance consistency through Token Merging (ToMe) [76], [77]. It partitions video frames into chunks and applies inter-frame ToMe within each chunk to reduce the number of self-attention layers input tokens. To ensure long-term consistency, a set of cross-chunk global tokens is maintained, merging with and being updated by each chunk. VidToMe is compatible with various image editing approaches, such as ControlNet [54] and PnP [14].

### 3.1.2 Structure Conditioning

One primary challenge in video editing is the occurrence of temporal instability, often resulting in distortions in the shapes of objects. Many recent works explicitly use structural representations to address this issue.

**Depth Maps and Bounding Boxes.** Gen-1 [94] concatenates depth maps [171] with the noisy latents  $\mathbf{z}_t$  as inputs to the noise predictor, effectively offering sequential structure guidance. Nevertheless, a major limitation of Gen-1 is the high computational cost involved in fine-tuning all parameters for video data. To address this limitation, MagicEdit [156] freezes the pre-trained parameters of the T2I model and fine-tunes the new temporal layers on video data, similar to AnimateDiff [20]. Subsequently, it directly integrates the ControlNet [54] trained for conditional image generation. The integrated model demonstrates capabilities in video stylization, local editing, conceptual mixing, *etc.*

Ground-A-Video [157] utilizes depth maps to offer spatial control through an inflated ControlNet [54]. Moreover, Ground-A-Video integrates bounding boxes to explicitly define the regions that should remain unedited. The bounding boxes from GLIP [172] are encoded as supplementary key-value features within cross-attention and temporal self-attention layers.

**Appearance Conditions.** During training, the model inadvertently memorizes appearance information from the source video, resulting in unexpected visual elements in the edited videos. To address this challenge, LAMP [158] proposes editing the first frame using off-the-shelf image editing methods [46], [54]. Then, the edited frame, along with other frames, is input into the denoising model, effectively decoupling appearance and motion from the learning pro-

cess. LAMP [158] also proposes the use of spatio-temporal convolution layers to enhance temporal consistency:

$$\text{ST-Conv}(\mathbf{h}) = \text{Sigmoid}(\text{S-Conv}(\mathbf{h})) \odot \text{T-Conv}(\mathbf{h}), \quad (23)$$

where  $\mathbf{h} \in \mathbb{R}^{d \times F \times W \times H}$  represents the hidden feature, with S-Conv( $\cdot$ ) and T-Conv( $\cdot$ ) operating on its  $d \times W \times H$  and  $d \times F$  dimensions, respectively. And  $\odot$  denotes the element-wise multiplication. During inference, LAMP adopts a shared latent state initialization strategy [173] to enhance consistency. Specifically, it samples a shared anchor latent state  $\mathbf{z}_T^{\text{anchor}} \sim \mathcal{N}(\mathbf{0}, \mathbf{I})$ . Each frame’s latent states are obtained by interpolating between the shared anchor latent and a Gaussian random variable,  $\mathbf{z}_T^f = \alpha \mathbf{z}_T^{\text{anchor}} + (1 - \alpha) \mathbf{z}^f$ , where random variable  $\mathbf{z}^f \sim \mathcal{N}(\mathbf{0}, \mathbf{I})$  and  $\alpha$  is a hyperparameter to control the degree of correlation.

CCEdit [159] adopts a trident-like architecture: an inflated T2I UNet with temporal layers and two separate hyper-networks [54], [55] dedicated to structure and appearance. An anchor frame from the source video is edited into  $\mathbf{z}_0^{\text{anchor}}$  by the I2I method before being fed into the appearance hyper-network to extract pyramid features. These appearance features are subsequently added to the UNet [55] encoder blocks. This design facilitates the propagation of the edited anchor frame throughout the video. Similarly, the structural features are extracted by another hyper-network and incorporated into the decoder of the denoising UNet to provide structural guidance [54]. For inference, the latent state for each frame  $\mathbf{z}_T^f$  is independently initialized from  $\mathcal{N}(\alpha \mathbf{z}_0^{\text{anchor}}, \mathbf{I})$  rather than  $\mathcal{N}(\mathbf{0}, \mathbf{I})$ . This approach enables the anchor frame to contribute a portion of low-frequency information, adjusted by a small factor  $\alpha$ .

**Motion Conditions.** Despite being equipped with temporal self-attention layers, preliminary experiments revealed a deficiency of temporal smoothness [160]. MoCA [74] and FlowVid [160] integrate the edited first frame and optical flow [117] into the model input. Specifically, MoCA converts the optical flow into RGB frames and channel-wisely concatenates it with the edited first frame  $\mathbf{z}_0^1$  and intermediate noisy latents  $\mathbf{z}_t$ . Conversely, FlowVid utilizes the source optical flow  $\mathcal{F}^{1 \rightarrow f}$ , the warpings of the edited first frame  $\mathcal{F}^{1 \rightarrow f}(\mathbf{z}_0^1)$ , and occlusion masks  $\mathcal{O}^{1 \rightarrow f}$ . Here, the optical flow operations are denoted in Section 2.3.2. Moreover, FlowVid integrates a ControlNet-like architecture [54] with depth maps [171] and optical flows [117] conditions.

VideoComposer [161] extends the types of controllable conditions and provides simultaneous control with multiple conditions, including sketch images [174], depth maps [171], and motion vectors [114]. It employs Spatio-Temporal Condition (STC) encoders, consisting of spatial convolution layers followed by temporal transformer layers. The multimodal conditions from STC encoders are aggregated through element-wise addition and concatenated with the noisy latent state  $\mathbf{z}_t$  along the channel dimension, facilitating collaborative control.

VideoControlNet [162], proposed by Hu & Xu, demonstrates video editing using T2I diffusion models [54] and optical flow [117] without parameter tuning. The first frame is edited using ControlNet [54] with Canny or depth controls. Then it divides subsequent frames into groups of size  $g$ , where the last frame of each group is generated by warping the previous edited frame with dense optical



flow  $\mathcal{F}^{f \rightarrow f+g}(\mathbf{x}^f)$  and refining the occlusions through pre-trained inpainting model [54]. Finally, the intermediate frames are generated by bidirectionally warping the adjacent edited frames.

### 3.1.3 Training Modification

Supervision plays a crucial role in tuning-based methods. Various supervision training proposed specifically for video editing has demonstrated good results.

**Motion-Oriented Loss.** MotionDirector [36] decouples the appearance and motion learning as AnimateDiff [20]. Specifically, it first optimizes the spatial layers using LoRAs [75]. Then, it combines the trained LoRAs from the first stage and optimizes the LoRAs of the temporal attention blocks. To mitigate appearance bias, it introduces a residual operation:

$$\delta(\epsilon^f) = \sqrt{1 + \beta^2} \epsilon^f - \beta \epsilon^{\text{anchor}}, \quad (24)$$

where the  $\epsilon^{\text{anchor}}$  is randomly selected from  $\{\epsilon^f\}_{f=1}^F$  during training and  $\beta$  serves as the decentralization factor. The residual operation is used to formulate a debiased temporal loss by substituting the  $\epsilon$  from Equation (7) into  $\delta(\epsilon)$ :

$$\mathcal{L}_{\text{debiased}} = \mathbb{E}[\|\delta(\epsilon_t) - \delta(\epsilon_\theta(\mathbf{z}_t, t, y))\|_2^2]. \quad (25)$$

During the optimization stage of temporal LoRAs, MotionDirector combines Equations (7) and (25)  $\mathcal{L}_{\text{MotionDirector}} = \mathcal{L}_{\text{simple}} + \mathcal{L}_{\text{debiased}}$  as the final loss function. Similarly motivated, VMC [151] defines a residual operation with a pre-defined stride:  $\delta(\epsilon^f) = \epsilon^{f+\text{stride}} - \epsilon^f$ . Their empirical design opts for cosine similarity  $S_{\text{cos}}(\mathbf{a}, \mathbf{b}) = 1 - \langle \frac{\mathbf{a}}{\|\mathbf{a}\|_2}, \frac{\mathbf{b}}{\|\mathbf{b}\|_2} \rangle$  over the Euclidean distance to optimize the temporal attention layers:

$$\mathcal{L}_{\text{VMC}} = \mathbb{E}[S_{\text{cos}}(\delta(\epsilon_t), \delta(\epsilon_\theta(\mathbf{z}_t, t, y)))] \quad (26)$$

**Image-Video Mixed Fine-tuning.** Dreamix [152] fine-tunes a pre-trained T2V model, Imagen Video [18], using a combination of frames and video segments extracted from the source video. This hybrid training approach ensures the preservation of both structure and motion characteristics. Besides, Dreamix adopts the SDEdit [61] schema, which initiates the sampling process by adding noise to the source video to perturbate its high-frequency structures.

**Textural Embedding Fine-tuning.** Many approaches choose to finetune the feature embeddings that directly reflect semantic information. SAVE [153] expands upon the concept of textural inversion [66], [67] by introducing separate sets of token embeddings for appearance and motion. The optimization begins by learning the token embeddings representing appearance information. Subsequently, SAVE focuses on optimizing the time-variant motion token embeddings, facilitating a disentangled learning process:  $\tau_{\text{motion}} = \mathbf{W} \cdot \mathcal{P}(\tau_{\text{motion}})$ , where  $\tau_{\text{motion}} \in \mathbb{R}^{d_\tau \times F \times L}$  represents the expanded motion embedding. It is initialized by duplicating the original tokens along the temporal dimension to achieve rapid coverage.  $\mathcal{P}(\cdot)$  represents temporal positional encoding. While optimizing the motion tokens, SAVE employs a cross-attention map-based regulation to prevent overspreading [15].

**Instruction-Based Fine-tuning.** An inherent limitation of description-based methods is requiring users to provide both source and target prompts, necessitating a text-video

paired dataset format. Beyond the increased workload, user descriptions of non-editing areas occasionally impact overall quality. Pioneering works in image editing [16] have introduced methods requiring only a single editing instruction, significantly enhancing efficiency. Researchers have extended this approach to video editing.

InstructVid2Vid [154], proposed by Qin *et al.*, formulates this task as a supervised learning problem and introduces a data curation pipeline. Firstly, BLIP [175] generates captions for the source videos. These captions are utilized to generate target captions and editing instructions using ChatGPT [176]. Subsequently, the source videos, source captions, and target captions are leveraged by off-the-shelf editing methods like Tune-A-Video [163] to produce the target video. New triplet samples include editing instructions, source videos, and edited videos. They are used to train the instruction-based video editing model. InstructVid2Vid also incorporates a delta-frame regularization  $\mathcal{L} = \mathcal{L}_{\text{simple}} + \alpha \sum_{f=2}^F (\epsilon^f - \epsilon^{f-1})$  to maintain consistency between consecutive frames. During inference, the additional preprocessing steps, such as per-video fine-tuning or latent inversion, are no longer needed, thereby enhancing efficiency.

Instead of collecting videos, InsV2V [164] initiates by constructing prompts [16], [177]. It employs a T2V model [80] and P2P [13] to generate the source and target videos from prompts. It focuses on editing long videos. Simply splitting a long video into non-overlapping chunks of size  $F$  and processing each chunk individually results in visible boundaries between chunks. InsV2V introduces a motion compensation approach to address this issue. It appends the last  $a$  frames from the  $(i-1)$ -th chunk  $\mathbf{z}_t^{f-a:f-1}(i-1)$  into the input of  $i$ -th chunk  $\mathbf{z}_t^{f:f+F}(i)$  and predicts  $[\epsilon_\theta^{f-a:f-1}(i-1), \epsilon_\theta^{f:f+F}(i)]$ . Subsequently, the prediction discrepancies are corrected:

$$\epsilon_\theta^{f:f+F}(i) \leftarrow \epsilon_\theta^{f:f+F}(i) + \frac{1}{a} \sum_{j=1}^a (\epsilon_\theta^{f-j}(i-1) - \epsilon_\theta^{f-j}(i)). \quad (27)$$

## 3.2 Attention Feature Injection

The hidden features in diffusion models inherently capture semantic correspondence [63]. Analogous to image editing feature injection techniques (discussed in Section 2.2.2), manipulating hidden features to edit a video is a promising direction. We classify related methods into two categories based on the origination of the injected hidden features.

### 3.2.1 Inversion-Based Feature Injection

Hidden features derived from the reconstruction branch can facilitate the generation of the target video. Furthermore, recognizing that videos inherently encompass spatio-temporal information, some methods [149], [150] utilize multiple branches to manage this complexity effectively.

**Dual-Branch.** Video-P2P [144] and Vid2Vid-Zero [145] expand the P2P [13] framework into the realm of video editing. They both employ cross-attention map injection [13] and null-text inversion [62], as discussed in Section 2.2.2. The null-text embeddings are shared across all frames to enhance semantic consistency and reduce memory usage. Video-P2P replaces spatial self-attention layers with

sparse-causal attention, introduces temporal attention layers, and implements one-shot tuning to learn temporal consistency [163]. Vid2Vid-Zero, on the other hand, highlights the necessity of global spatio-temporal attention layers, with key and value features sourced from all frames. Even without parameter tuning, its inflated 2D layers empirically demonstrate effective performance for bi-directional temporal modeling.

Fate-Zero [146] injects both cross-attention and self-attention maps, reaping the benefits from P2P [13] and PnP [14]. The fusion masks for self-attention injection are generated by binarizing the cross-attention maps [64], [65]. Edit-A-Video [147] has a similar attention map injection schema as Fate-Zero and uses null-text inversion [62] to mitigate errors associated with latent inversion and classifier-free guidance [49]. Additionally, it interpolates the fusion masks between the first frame and the current frame, weighted by self-attention maps, thereby ensuring temporal smoothness in the edited area.

Make-A-Protagonist [148] follows the path of PnP [14] and MasaCtrl [15], injecting the latent features in residual blocks and self-attention maps from the reconstruction branch into the editing branch. Rather than deriving the mask from attention maps as in prior works [15], it utilizes Grounded SAM [178] to obtain the first frame segmentation mask and Xmem [179] to propagate it for precise fusion.

**Multiple Branches.** UniEdit [149] and AnyV2V [150] disentangle appearance and motion injection by introducing two auxiliary branches: a reconstruction and a motion-reference branch. All branches are initialized by pre-trained video generation models [83], [97], [98], [101]. The reconstruction branch injects spatial self-attention query and key features at earlier sampling steps to maintain structural consistency. Furthermore, spatial self-attention value features from the reconstruction branch are selectively injected to preserve non-edited regions. The motion-reference branch contributes to the desired motion by injecting only its temporal self-attention query and key features, thereby avoiding potential structural instability. Although sharing the injection workflow, UniEdit and AnyV2V diverge in the base models. UniEdit leverages a T2V model, LaVie [83], and efficiently incorporates text prompts. AnyV2V utilizes I2I experts [16], [180], [181], [182] to edit the first frame, and subsequently applies a video editing pipeline based on pre-trained I2V models [97], [98], [101] to enhance compatibility across a wide range of editing tasks.

### 3.2.2 Motion-Based Feature Injection

Feature injection can also occur across frames. The intrinsic motion information within the source video provides valuable prior knowledge for indicating temporal correspondence and guiding inter-frame feature injection.

TokenFlow [34] uses inter-frame feature similarity. It first processes several sampled keyframes by replacing spatial self-attention with a global spatio-temporal self-attention mechanism. TokenFlow then identifies the nearest neighbor from adjacent keyframes for each token. For a token at frame  $f$  with spatial coordinates  $(x_f, y_f)$ , its nearest neighbor tokens at adjacent past keyframe  $f-$  and adjacent future keyframe  $f+$  are denoted as  $(x_{f-}, y_{f-})$  and  $(x_{f+}, y_{f+})$ ,

respectively. Subsequently, each frame is independently denoised with inter-frame feature injection:

$$\mathbf{h}_{[x_f, y_f]}^f \leftarrow \alpha_f \mathbf{h}_{[x_{f-}, y_{f-}]}^{f-} + (1 - \alpha_f) \mathbf{h}_{[x_{f+}, y_{f+}]}^{f+}. \quad (28)$$

where  $\alpha_f \in (0, 1)$  is a scalar proportional to the distance between frame  $f$  and its adjacent keyframes  $j\pm$ . And  $\mathbf{h}$  denotes the intermediate hidden features output by the self-attention layers.

In contrast to the feature similarity-based approach in TokenFlow, FLATTEN [33] selects injected features based on optical flow. Specifically, for a token  $\mathbf{x}_{[x_1, y_1]}^{s1}$  at the first frame of the source video  $\mathbf{x}^{s1}$  with spatial coordinates  $(x_1, y_1)$ , optical flow estimation methods [183] can track its spatial correspondence across the remaining  $F - 1$  frames, denoting it as a trajectory:

$$\mathcal{T}(\mathbf{x}^s, x_1, y_1) = \{\mathbf{x}_{[x_1, y_1]}^{s1}, \dots, \mathbf{x}_{[x_F, y_F]}^{sF}\}. \quad (29)$$

During editing, its temporal-guided attention mechanism pairs a query token with key and value tokens from the same trajectory in other frames:

$$\begin{aligned} \mathbf{Q}_{[x_f, y_f]}^f &= \mathbf{h}_{[x_f, y_f]}^f, \\ \mathbf{K}_{[x_f, y_f]}^f &= \mathbf{V}_{[x_f, y_f]}^f = \mathcal{T}(\mathbf{h}, x_1, y_1) \setminus \{\mathbf{h}_{[x_f, y_f]}^f\}. \end{aligned} \quad (30)$$

It is important to note that temporal-guided attention does not involve positional encoding, projection matrices, or feed-forward layers, making seamless integration without additional training.

FRESCO [143] follows a similar approach to FLATTEN, with additional steps to refine the value features. It performs one forward and reverse DDPM [39] step on a source frame  $\mathbf{z}^{sf}$ , and extracts its query features  $\mathbf{Q}^{sf} \in \mathbb{R}^{d \times N}$  and key features  $\mathbf{K}^{sf} \in \mathbb{R}^{d \times N}$ . FRESCO then introduces a spatial-guided attention mechanism, utilizing these features to reweight the query features in the editing video:

$$\mathbf{Q}^f \leftarrow \text{Softmax}\left(\frac{(\mathbf{Q}^{sf})^T \cdot \mathbf{K}^{sf}}{\lambda \sqrt{d}}\right) \cdot \mathbf{Q}^f, \quad (31)$$

where  $\lambda$  is a scaling factor. Subsequently, it utilizes the efficient cross-frame attention to enhance the value features with cross-frame information:

$$\mathbf{V}^f \leftarrow \text{Softmax}\left(\frac{(\mathbf{Q}^f)^T \cdot \mathbf{K}_{[\mathbf{p}]}}{\sqrt{d}}\right) \cdot \mathbf{V}_{[\mathbf{p}]}. \quad (32)$$

Here,  $\mathbf{p}$  denotes a set of attended coordinates: all coordinates in the first frame are included, and subsequent frames only include previously non-observed areas. The refined value features are utilized in a temporal-guided attention mechanism, similar to FLATTEN [33] in Equation (30). Moreover, it finetunes the input features of each decoder layer. The source and edited video undergo one DDPM [39] forward and inverse step. The input features at the  $f$ -th frame of source and target video in the inverse process are denoted as  $\mathbf{h}^{sf} \in \mathbb{R}^{d \times N}$  and  $\mathbf{h}^f \in \mathbb{R}^{d \times N}$ , respectively. These

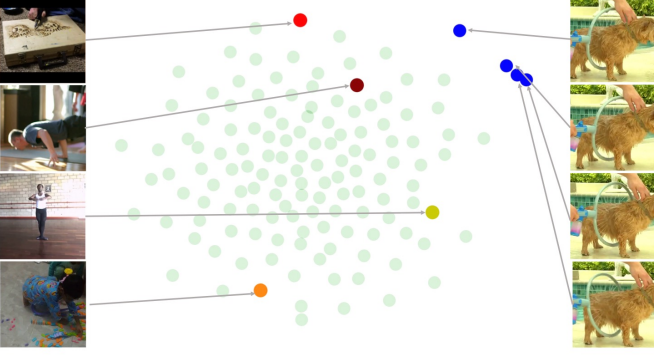


Fig. 8. The t-SNE visualization illustrates the distribution of  $\mathbf{z}_T$ . The samples are obtained from latent inversion on real video frames using a pre-trained T2I diffusion model. The green dots in the background represent samples drawn from i.i.d. Gaussian distribution for reference. Blue dots represent successive frames from the same video, clustered closely together. While frames from different videos (yellow and red dots) are scattered and exhibit no correlation. The plot is adapted from PYoCo [173].

feature embeddings are optimized by minimizing a spatio-temporal alignment loss:

$$\begin{aligned} \mathcal{L} &= \mathcal{L}_{\text{temporal}} + \lambda \mathcal{L}_{\text{spatial}}, \\ \mathcal{L}_{\text{temporal}} &= \sum_{f=1}^{F-1} \|\mathcal{O}^{f \rightarrow f+1}(\mathbf{h}^{f+1} - \mathcal{F}^{f \rightarrow f+1}(\mathbf{h}^f))\|_1, \\ \mathcal{L}_{\text{spatial}} &= \lambda \sum_{f=1}^F \|\mathbf{h}^{sf^T} \cdot \mathbf{h}^{sf} - \mathbf{h}^{f^T} \cdot \mathbf{h}^f\|_2^2, \end{aligned} \quad (33)$$

where  $\lambda$  is a scaler used to strike the balance.

### 3.3 Diffusion Latent Manipulation

It is commonly hypothesized that the diffusion process operates independently of other design components [50], such as network architecture and training configuration. From the perspective of the diffusion process, the noise predictor can be treated as a black box [50], [184], [185]. This section reviews diffusion latent states initialization and transition technologies for video editing.

#### 3.3.1 Latent Initialization

As shown in Figure 8, the initial latent states  $\mathbf{z}_T$  from consecutive video frames demonstrate significant correlation. Simply extending the image latent state initialization to video results in suboptimal performance [140]. While latent inversion methods [46], [62] provide a solution, they require additional sampling steps for each source video. On the other hand, methods such as LAMP [158] and CCEdit [159] employ simple initialization strategies to achieve satisfactory performance, underscoring the significance of latent state initialization in video diffusion models.

Chen’s Control-A-Video [140] proposes a residual-based latent state propagation approach:

$$\mathbf{z}_T^f = \alpha^f \mathbf{z}_T^{f-1} + (1 - \alpha^f) \nu, \quad (34)$$

where  $\alpha^f = |\mathbf{x}^f - \mathbf{x}^{f-1}| < \mathcal{R}$  serves as the mask to ensure that unchanged areas exhibit the same initialization,  $\mathcal{R}$  represents a pre-defined threshold, and  $\nu \sim \mathcal{N}(\mathbf{0}, \mathbf{I})$  is

a standard Gaussian random variable. Similarly motivated, the initialization of Ground-A-Video [157] is also formulated as Equation (34) with a little difference:  $\alpha^f = |\mathcal{F}^{f-1 \rightarrow f}| < \mathcal{R}$ . Chen *et al.* [140] also introduces a flow-based latent state initialization scheme:

$$\mathbf{z}_T^f = \mathcal{F}^{f-1 \rightarrow f}(\mathbf{z}_T^{f-1}). \quad (35)$$

Here, the optical flow operation  $\mathcal{F}$  is defined in Section 2.3.2.

Text2Video-Zero [141] constructs the inter-frame linkage of latent states in an earlier diffusion step  $T' = T - \Delta T$ , in contrast to Chen *et al.* [140], which does so at step  $T$ . It begins by randomly initializing the first frame  $\mathbf{z}_{T'}^1 \sim \mathcal{N}(0, I)$ , followed by  $\Delta T$  denoising steps to obtain  $\mathbf{z}_{T'}^1$ . Text2Video-Zero subsequently defines a sequence of translation vectors for each frame  $\delta^f = (\delta_x^f, \delta_y^f) \in \mathbb{R}^2$ . These translation vectors are employed to warp the first frame  $\mathbf{z}_{T'}^1$  into the subsequent frames  $\mathbf{z}_{T'}^f \leftarrow \mathbf{z}_{T'}^1 + \delta_x^f \cdot \mathbf{e}_x + \delta_y^f \cdot \mathbf{e}_y$ . This warping can be optionally disabled in specific areas indicated by off-the-shelf object detection bounding boxes [186], preserving the consistency of the background.

Rather than manual construction, Chu’s VideoControlNet [142] optimizes the inter-frame correlation with optical flow supervision:

$$\mathcal{L} = \sum_{f=1}^F \left( \frac{1}{f} \sum_{a=1}^f \mathcal{O}^{a \rightarrow f} \odot (\epsilon_\theta(\mathbf{z}_T^f) - \epsilon_\theta(\mathcal{F}^{a \rightarrow f}(\mathbf{z}_T^a))) \right), \quad (36)$$

where  $\epsilon_\theta(\cdot)$  is a pre-trained T2I ControlNet [54],  $\odot$  represents the element-wise multiplication. The optical flow operation is defined in Section 2.3.2. Chu *et al.* also suggests first optimizing keyframes and then interpolating the remaining frames to accelerate the optimization.

#### 3.3.2 Latent Transition

Enhancing the reverse latent transition (denoising) process aids the convergence of  $\{\mathbf{z}_t\}_{t=T}^0$  towards a temporally consistent video distribution. Pix2Video [35] demonstrates inter-frame smoothness via gradient descent. Rather than the routine reverse diffusion sampling step as described in Equation (10), it updates the latent states by:

$$\mathbf{z}_{t-1}^f \leftarrow \mathbf{z}_{t-1}^f - \lambda_t \nabla_{\mathbf{z}_t^f} \|\mathbf{z}_{t \rightarrow 0}^{f-1} - \mathbf{z}_{t \rightarrow 0}^f\|_2, \quad (37)$$

where  $\lambda_t$  represents the step size, and  $\mathbf{z}_{t \rightarrow 0}^f$  denotes the estimated  $\mathbf{z}_0^f$  as defined in Equation (9). This guidance prevents temporal inconsistency at each denoising step.

ControlVideo [137], proposed by Zhang *et al.*, enforces the smoothness of the  $\mathbf{z}_{t \rightarrow 0}$  as defined in Equation (9). Each middle frame is interpolated using its two adjacent frames:

$$\mathbf{z}_{t \rightarrow 0}^f \leftarrow \mathcal{E} \left( \text{Interpolate}(\mathcal{D}(\mathbf{z}_{t \rightarrow 0}^{f-1}), \mathcal{D}(\mathbf{z}_{t \rightarrow 0}^{f+1})) \right). \quad (38)$$

Here, the interpolated frames  $f \in \{f_0, f_0 + 2, \dots\}$  are sampled in an interleaved manner, with  $f_0 \in \{0, 1\}$ . The functions  $\mathcal{E}(\cdot)$  and  $\mathcal{D}(\cdot)$  represent the VAE encoding and decoding. Subsequently, Equation (10) is utilized to update the diffusion states. The interpolation frames are updated with  $f_0 \leftarrow 1 - f_0$  after each denoising step. The sequential combination of two steps effectively smooths all frames.

Rerender-A-Video [138] exhibits inter-frame fusion in both VAE latent space and pixel space, ensuring simultaneous consistency in semantics and texture. The latent fusion

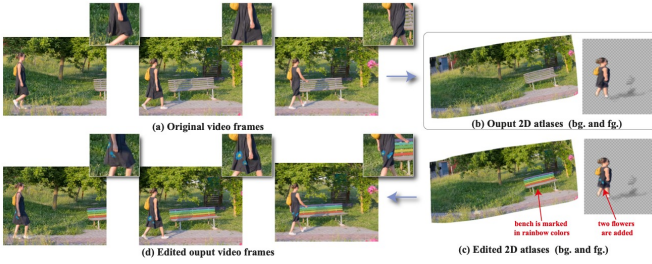


Fig. 9. Layered Neural Atlases (LNA) [135]. Original video frames are mapped to flattened 2D atlases by warping models. Edits on the 2D atlases can be propagated to all frames of the video. The plot is adapted from LNA [135].

is achieved by updating  $\mathbf{z}_{t \rightarrow 0}$  (defined in Equation (9)) using the warped first frame  $\mathcal{F}^{1 \rightarrow f}(\mathbf{z}_{t \rightarrow 0}^1)$  and its corresponding occlusions  $\mathcal{O}^{1 \rightarrow f}$ :

$$\mathbf{z}_{t \rightarrow 0}^f \leftarrow \mathcal{O}^{1 \rightarrow f} \mathbf{z}_{t \rightarrow 0}^f + (1 - \mathcal{O}^{1 \rightarrow f}) \mathcal{F}^{1 \rightarrow f}(\mathbf{z}_{t \rightarrow 0}^1), \quad (39)$$

where the optical flow is estimated from the source video. The fusion in the VAE latent space only occurs during the early denoising steps. To enhance low-level feature consistency, the first-round denoising output  $\hat{\mathbf{x}}$  is successively fused with the previous frame and the first frame:

$$\begin{aligned} \hat{\mathbf{x}}^f &\leftarrow \mathcal{O}^{f-1 \rightarrow f} \hat{\mathbf{x}}^f + (1 - \mathcal{O}^{f-1 \rightarrow f}) \mathcal{F}^{f-1 \rightarrow f}(\hat{\mathbf{x}}^{f-1}), \\ \hat{\mathbf{x}}^f &\leftarrow \mathcal{O}^{1 \rightarrow f} \hat{\mathbf{x}}^f + (1 - \mathcal{O}^{1 \rightarrow f}) \mathcal{F}^{1 \rightarrow f}(\hat{\mathbf{x}}^1). \end{aligned} \quad (40)$$

Within the occlusion mask area  $\mathcal{O}^f = \mathcal{O}^{1 \rightarrow f} \cap \mathcal{O}^{f-1 \rightarrow f}$ , the frame  $\hat{\mathbf{x}}^f$  remains unaltered. Subsequently, Rerender-A-Video regenerates the edited video with the guidance of  $\hat{\mathbf{x}}$  at each denoising step:

$$\hat{\mathbf{z}}_{t-1}^f \leftarrow \mathcal{O}^f \mathbf{z}_{t-1}^f + (1 - \mathcal{O}^f) \hat{\mathbf{z}}_{t-1}, \quad (41)$$

where  $\hat{\mathbf{z}}_{t-1}$  is obtained by applying Equation (3) on  $\hat{\mathbf{z}}_0 = \mathcal{E}(\hat{\mathbf{x}})$ . Note that latent space fusion (shown in Equation (39)) occurs before Equation (10), while the second-round pixel space fusion (shown in Equation (41)) occurs after it.

RAVE [139] employs a ‘grid trick’: video frames are divided into  $g$  equal-sized groups. Frames within the same group are concatenated along spatial dimensions into a large grid image as the input of the pre-trained I2I diffusion model [14], [54]. The frames within each grid maintain a certain level of consistency. After each denoising step, the frames are randomly permuted into different groups, enabling interaction with more frames. Over the  $T$  denoising steps, each frame can interact with up to  $T(g-1)$  other frames, promoting global consistency. Such grid manipulation requires neither additional parameters nor extra training, resulting in an efficient video editing adaptation.

### 3.4 Canonical Representation

The aforementioned methods represent the video clips as image frames. This section focuses on the video canonical representations, also known as atlases. The canonical atlas can effectively handle the temporal axis of video data and bridge the gap between video and image modalities. This representation has inspired the adaptation of image editing methods for video applications. More recently, as diffusion models have shown remarkable abilities in image

editing [29], researchers have integrated video canonical representations with diffusion models to improve video editing. We begin with an introduction to video neural canonical representations, followed by introducing related video editing methods.

#### 3.4.1 Atlas Learning

As shown in Figure 9, the seminal work Layered Neural Atlases (LNA) [135] encodes a video pixel  $\mathbf{x}_{[x,y]}^f \in \mathbb{R}$  to an atlas pixel  $\mathbf{a}_{[u,v]} \in \mathbb{R}$  by learning the transformation from video voxel to atlas coordinates  $(u, v) = \mathcal{W}(x, y, f) \in \mathbb{R}^2$ .  $\mathcal{W}(\cdot)$  represents the warping network, indicating the many-to-one mapping from 3D voxels to 2D atlas coordinates. Specifically, it considers two separate atlases,  $\mathbf{a}^{\text{FG}}$  and  $\mathbf{a}^{\text{BG}}$ , and two warping networks,  $\mathcal{W}^{\text{FG}}(\cdot)$  and  $\mathcal{W}^{\text{BG}}(\cdot)$ , for foreground and background objects, respectively. To demonstrate self-supervised learning, LNA designs a reconstruction process using a color prediction network  $\mathcal{X}(\cdot)$  and an opacity prediction network  $\mathcal{A}(\cdot)$ . The video reconstruction from the atlas is defined by:

$$\hat{\mathbf{x}}_{[x,y]}^f = \alpha \mathcal{X}(u^{\text{FG}}, v^{\text{FG}}) + (1 - \alpha) \mathcal{X}(u^{\text{BG}}, v^{\text{BG}}), \quad (42)$$

where  $\mathcal{X}(u, v)$  represents the predicted RGB value at atlas coordinate  $(u, v)$  and  $\alpha = \mathcal{A}(x, y, f) \in [0, 1]$  represents the blending factor of the predicted colors at voxel  $(x, y, f)$ . During training, the warping network  $\mathcal{W}(\cdot)$ , the color prediction network  $\mathcal{X}(\cdot)$ , and the opacity prediction network  $\mathcal{A}(\cdot)$  are trained together on the source video using a reconstruction loss with rigidity regularizations to maintain. Once the video is registered through training, edits can be applied directly to the canonical atlas. The learned 2D-to-3D coordinates mapping  $\mathcal{W}(\cdot)$  acts as the translation mechanism between the atlas and the video frames. The color prediction network  $\mathcal{X}(\cdot)$  is not involved during the editing stage.

Although the effective representation of LNA can guarantee temporal consistency by design, it requires significant preprocessing time for each video, generally taking hours of training. CoDeF [136] addresses this by proposing an effective hash-based architecture for warping and reconstruction. It uses pre-trained SAM-tracking [187] to derive the blending  $\alpha$  values rather than learning them to reduce complexity. CoDeF also distills trajectory information from optical flow [117] to enhance consistency. The resulting atlas serve as an effective canonical representation for video editing.

#### 3.4.2 Atlas Editing

Editing the canonical atlases and then propagating the edits to the entire video offers the convenience of maintaining temporal consistency. However, the contents in the canonical atlas diverge from the distribution of natural images. Directly applying image editing methods trained on natural images may lead to unexpected deteriorated regions or semantic deformations [133].

VidEdit [133] focuses on editing foreground objects using extracted structural information to guide the editing process. It applies the semantic segmentation method [188] to delineate the region of interest during editing precisely. Additionally, it employs SDEdit [61] with HED [189]

conditions to provide critical structural guidance, thereby avoiding the pitfall of atlas distortion. On the other hand, DiffusionAtlas [134] fine-tunes a pre-trained T2I diffusion model [5] to adapt the atlas distribution. Atlas editing is demonstrated by generating editing prompts starting from the DDIM inverted latent states [46]. Additionally, DiffusionAtlas trains the foreground warping network  $\mathcal{W}^{\text{FG}}(\cdot)$  and the opacity prediction network  $\mathcal{A}(\cdot)$  on the edited atlases to map the edited atlas back to video frames.

### 3.4.3 Edit Propagation

Another promising solution to address the issue of unnatural atlas distortion is to edit video frames and propagate these edits throughout the video using canonical atlases. StableVideo [131] starts by editing several keyframes. Specifically, the first keyframe is edited with structural conditions [54] and then warped into a partially edited atlas. It is worth noting that the atlas pixels not present in the first keyframe remain unmodified. The subsequent keyframes are initialized using their previous partially edited atlases and then undergo the SDEdit [61] to complete editing. Finally, an aggregation network trained on the source video frames and atlases is applied to combine these partially edited atlases into a fully edited atlas.

One challenge of using the pre-trained warping network  $\mathcal{W}(\cdot)$  is shape editing. Lee *et al.* [132] proposes propagating shape correspondences between source and target objects through the canonical atlas to achieve shape-aware video editing. They edit a keyframe using StableDiffusion [5]. Lee *et al.* estimates semantic correspondences [190] and represents them as a set of deformation vectors. Initially, the edited object is deformed to match the shape of its source object and propagates throughout the entire video. Simultaneously, the deformation vectors propagate throughout the video, bridging through the canonical space. These deformation vectors then restore the edited object shapes. Finally, it fine-tunes the foreground atlas network to enhance the visual quality of the edited frames.

## 3.5 Novel Conditioning

In addition to text prompts, the newly proposed handle point prompts enhance the controllability of interactive video editing. Furthermore, we also cover domain-specific methods that elucidate human action videos and leverage pose conditions in this section.

### 3.5.1 Point Conditioning

The expressiveness of text prompts is inherently limited by language modality. Can editing be controlled by clicking on a frame to move, add, remove, or replace objects? Interactive point-based editing has emerged as a novel conditioning method that provides flexible, precise, and generalized control [191]. Users can select handle and target points to move, add, or remove them. Edits applied to a single frame should propagate seamlessly across all frames.

**DragGAN and DragDiffusion.** The seminal point-based image editing work, DragGAN [191], operates on the StyleGAN2 [192] hidden features  $\mathbf{h} \in \mathbb{R}^{d \times W \times H}$  and includes two stages: motion supervision to enforce handle points  $\{\mathbf{p}_i\}$  to move towards target points  $\{\mathbf{t}_i\}$  and point tracking

to update the positions of the handle points  $\{\mathbf{p}_i\}$  after each movement step. In addition to the handle points, the motion supervision loss drives a surrounding patch  $\Omega(\mathbf{p}_i, r_1) = \{\mathbf{q} : \|\mathbf{q} - \mathbf{p}_i\| \leq r_1\}$  to move toward target points, taking the form:

$$\mathcal{L}_{\text{motion}} = \sum_i \sum_{\mathbf{q}_i \in \Omega(\mathbf{p}_i, r_1)} \|\mathbf{h}_{[\mathbf{q}_i + \mathbf{d}_i]} - \text{sg}(\mathbf{h}_{[\mathbf{q}_i]})\|_1, \quad (43)$$

where  $\mathbf{d}_i = (\mathbf{t}_i - \mathbf{p}_i) / \|\mathbf{t}_i - \mathbf{p}_i\|_2 \in [0, 1]^2$  is an unit vector pointing from  $\mathbf{p}_i$  to  $\mathbf{t}_i$ , and  $\text{sg}(\cdot)$  is the stop gradient operation. Moreover, DragGAN allows users to provide a binary mask  $\mathbf{M} \in \{0, 1\}^{d \times W \times H}$  to prevent movement in the masked areas. It introduces a reconstruction loss:

$$\mathcal{L}_{\text{reconstruction}} = \|(\mathbf{h} - \mathbf{h}_0) \odot (\mathbf{1} - \mathbf{M})\|_1, \quad (44)$$

where  $\mathbf{h}_0 \in \mathbb{R}^{d \times W \times H}$  denotes the initial hidden feature and  $\odot$  denotes the element-wise multiplication. After each optimization step, the position of handle points in the new hidden feature is unclear. The point tracking updates their position by searching over all neighbors around  $\mathbf{p}_i$ , formulated as:

$$\mathbf{p}_i \leftarrow \arg \min_{\mathbf{q}_i \in \Omega(\mathbf{p}_i, r_2)} \|\mathbf{h}_{[\mathbf{q}_i]} - \mathbf{h}_{[\mathbf{p}_i]}\|_1. \quad (45)$$

The optimization is iteratively applied to the new handle points until they reach the target points.

DragDiffusion [193] extends point-based image editing to diffusion models. It first performs sample-specific fine-tuning on the source image using LoRA [75]. Instead of operating on hidden features, it applies motion supervision to the latent states  $\mathbf{z}_t$  with the initial hidden state obtained from the latent inversion of the source image as described in Equation (18). As diffusion models exhibit greater generation diversity, DragDiffusion involves feature injection to retain attributes of the source image by injecting keys and values of the transformer blocks, as in MasaCtrl [15]. Concurrently, DragonDiffusion [194] provides training-free interactive manipulation using energy functions and a visual cross-attention design as alternative solutions. Free-Drag [195] enhances robustness through adaptive latent state updating and line search with backtracking.

**Point-Based Video Editing.** DragVideo [129] follows the DragDiffusion paradigm [193] and utilizes AnimateDiff [20] as a pre-trained video backbone. It requires user points and masks on the first and last frames. To propagate these conditions across frames, It employs Persistent Independent Particles (PIPs) [196] for the handle points, linear interpolation for the target points, and Track-Anything Model (TAM) [197] for the masks. Drag-A-Video [130] tracks the point and mask trajectories using diffusion hidden feature correspondence [63] instead of off-the-shelf models. It uses an averaged handle points feature across frames  $\overline{\mathbf{h}}_{[\mathbf{q}_i]} = \frac{1}{F} \sum_{f=1}^F \mathbf{h}_{[\mathbf{q}_i^f]}$  as supervision to enhance temporal consistency, with the motion loss formulated as:

$$\mathcal{L}_{\text{motion}} = \sum_{i,f} \sum_{\mathbf{q}_i^f \in \Omega(\mathbf{p}_i^f, r)} \|\mathbf{h}_{[\mathbf{q}_i^f + \mathbf{d}_i^f]} - \text{sg}(\overline{\mathbf{h}}_{[\mathbf{q}_i]})\|_1, \quad (46)$$

Moreover, Drag-A-Video optimizes the latent state across multiple timesteps using a shared latent state offset instead of focusing on a single timestep.

Unlike the above methods that use the DragDiffusion paradigm, VideoSwap [37] is inspired by the observation that semantic points can align the subject’s shape and motion trajectory. It extracts the DIFT [63] feature  $\mathbf{h}$  for each user-provided handle point  $\{\mathbf{p}_i\}$  and adds the MLP-projected DIFT feature to the corresponding position of the diffusion encoder [55]. These MLP projectors are trained on the diffusion loss in the surrounding region of the handle points  $\Omega(\mathbf{p}_i, r)$  as follows:

$$\mathcal{L} = \mathbb{E}_{t, \mathbf{z}_t, \epsilon_t, \mathbf{q}_i \in \Omega(\mathbf{p}_i, r)} \|(\epsilon_t - \epsilon_\theta(\mathbf{z}_t, t, \phi(\mathbf{h})))_{[\mathbf{q}_i]}\|_2^2, \quad (47)$$

where  $\phi(\cdot)$  indicates the trainable projection MLP. During inference, dropping the added encoder embeddings removes the subjects at a handle point. When moving handle points, VideoSwap utilizes the canonical atlas [135], as mentioned in Section 3.4, to track the trajectory of handle points and target points.

### 3.5.2 Pose Conditioning for Human Video Editing

Human video editing is a domain-specific task with substantial creative and commercial potential. It entails translating a source human video into another temporally coherent video, featuring the target character while replicating the source video actions. This task presents three challenges:

- **Temporal Consistency:** The inter-frame smoothness is a common challenge in video modeling.
- **Pose Alignment:** The edited video must adhere to the source poses.
- **Identity Alignment:** The target video should preserve the specified character’s identity.

Follow-Your-Pose [123] focuses on investigating the pose alignment and temporal consistency challenges. It utilizes the pose map, where vertices represent joints and edges denote limbs, as a domain-specific structural condition. This condition abstracts pose from the source video, maintaining only the structural information. Given the scarcity of high-quality annotated human action video datasets at that time, Follow-Your-Pose decouples temporal consistency and pose alignment learning. It first learns a pose-conditioned generative model using a pose-image dataset. Subsequently, it learns temporal consistency on videos without pose annotations. Specifically, pose maps are encoded using convolutional layers and integrated into pre-trained T2I UNet blocks [5] by addition. Follow-Your-Pose also incorporates temporal and sparse-causal attention mechanisms [163] to maintain temporal consistency. Only the newly added parameters are trained while the pre-trained parameters remain frozen. Once training is completed, these modules are combined to enable human video editing.

DreamPose [124] utilizes reference images to specify the character’s identity. Its reference image provides finer details than text prompts, such as facial and body attributes. Reference image embeddings from the image CLIP [198] and VAE [40] encoders are merged to capture intricate details and conditioned in the diffusion model using cross-attention. The pose conditions are concatenated with noisy latent states, expanding the input channels, as elaborated in Section 2.2. Moreover, it employs the hierarchical classifier-free guidance, as outlined in Equation (16).

DisCo [125] pre-trains its spatial layers on human image datasets [199], [200], [201], [202] to enhance identity

precision and integrates pose and background information through ControlNet [54]. MotionEditor [126] addresses ghosting and blurring effects caused by conflicting poses between the source video and the reference identity. Instead of directly adding ControlNet [54] outputs to the UNet, it uses a motion adapter before integration. This adapter includes two parallel paths: one employing temporal convolutions to enhance temporal pose sequence features, and the other incorporating cross-attention and temporal self-attention blocks. The cross-attention uses pose features to query UNet features, capturing correlated motion clues in noisy latent states.

MagicPose [127] enhances identity alignment by introducing an appearance branch. This branch is duplicated from the main branch and employed to extract identity features from the reference image. The self-attention key and value features of the main branch are augmented by concatenating with the appearance branch features:

$$\mathbf{T} = [\mathbf{W}_T \cdot \mathbf{h}, \mathbf{W}_T^r \cdot \mathbf{h}^r] \in \mathbb{R}^{d \times 2N}, \quad (48)$$

where  $\mathbf{T} \in \{\mathbf{K}, \mathbf{V}\}$ ,  $\mathbf{h} \in \mathbb{R}^{d \times N}$  represents the hidden features, and  $\mathbf{W}_T \in \mathbb{R}^{d \times d}$  represents the projection matrices from the main branch.  $\mathbf{h}^r \in \mathbb{R}^{d \times N}$  and  $\mathbf{W}_T^r \in \mathbb{R}^{d \times d}$  are their correspondence from the appearance branch. Similarly motivated, MagicAnimate [38] and AnimateAnyone [128] also incorporate the appearance branch. However, they distinguish themselves from MagicPose [127] by incorporating the hidden feature from the appearance branch and utilizing shared projection matrices:

$$\mathbf{T} = \mathbf{W}_T \cdot [\mathbf{h}, \mathbf{h}^r] \in \mathbb{R}^{d \times 2N}. \quad (49)$$

## 4 BENCHMARKING

With an increasing number of research studies, there is a growing need for a benchmark to evaluate and compare their strengths and limitations, aiding in selecting the most suitable method. Previous benchmarks either focus solely on text-to-video (T2V) or image-to-video (I2V) generation without video input [115], [116] or lack comprehensive evaluation across various dimensions [159], [203]. This section introduces V2VBench, a benchmark that quantitatively assesses video editing methods.

We start by introducing our curated video dataset in Section 4.1, followed by the evaluation metrics in Section 4.2. Finally, Section 4.3 presents the quantitative evaluation results and visualizations of the 16 methods.

### 4.1 Video Editing Dataset

#### 4.1.1 Source Videos

We collect 50 high-quality, open-licensed video clips from the internet as the source videos for V2VBench. These clips range from 2 to 100 seconds in length, with an average of 30 frames per second (FPS) and various aspect ratios, all with a minimum resolution of  $512 \times 512$  pixels. The videos are categorized into five common categories relevant to real

TABLE 1

V2VBench evaluation results. This table compares 16 diffusion-based text-guided video editing methods across 8 quality metrics. A higher score indicates better performance. † denotes that the method requires test-time tuning on the source video. ‡ denotes that the method requires pre-training on the video dataset. The methods are grouped by specific categories based on their main technological dependencies. The best results within each category are underlined, and the globally best metrics are highlighted in **bold font**.

	Method	Frames Quality	Video Quality	Semantic Consistency	Object Consistency	Frames Text Alignment	Video Text Alignment	Frames Pick Score	Motion Alignment
Network and Training Paradigm	Tune-A-Video [163]†	<u>5.001</u>	0.934	0.917	0.527	27.513	20.701	0.254	-5.599
	SimDA [165]†	4.988	0.940	0.929	0.569	26.773	20.512	0.248	-4.756
	VidToMe [167]	4.988	<u>0.949</u>	0.945	<u>0.656</u>	26.813	20.546	0.240	-3.203
	VideoComposer [161]‡	4.429	0.914	0.905	0.370	<u>28.001</u>	20.272	0.262	-8.095
	MotionDirector [36]†‡	4.984	0.940	<u>0.951</u>	0.617	27.845	<u>20.923</u>	<u>0.262</u>	<u>-3.088</u>
Attention Feature Injection	Video-P2P [144]†	4.907	0.943	0.926	0.471	23.550	19.751	0.193	-5.974
	Vid2Vid-Zero [145]	5.103	0.919	0.912	0.638	<u>28.789</u>	<u>20.950</u>	<u>0.270</u>	-4.175
	Fate-Zero [146]	5.036	<u>0.951</u>	<b>0.952</b>	0.704	25.065	20.707	0.225	<u>-1.439</u>
	TokenFlow [34]	5.068	0.947	0.943	<u>0.715</u>	27.522	20.757	0.254	-1.572
	FLATTEN [33]	4.965	0.943	0.949	0.645	27.156	20.745	0.251	-1.446
	FRESCO [143]†	<u>5.127</u>	0.908	0.896	0.689	25.639	20.239	0.223	-5.241
Diffusion Latents Manipulation	Text2Video-Zero [141]	5.097	0.899	0.894	0.613	<b>29.124</b>	20.568	0.265	-17.226
	Pix2Video [35]	5.075	0.946	0.944	0.638	28.731	<b>21.054</b>	<b>0.271</b>	-2.889
	ControlVideo [137]	<b>5.404</b>	<b>0.959</b>	<u>0.948</u>	0.674	28.551	20.961	0.261	-9.396
	Rerender [138]	5.002	0.872	0.863	<b>0.724</b>	27.379	20.460	0.261	-4.959
	RAVE [139]	5.077	0.926	0.936	0.664	28.190	20.865	0.255	<u>-2.398</u>

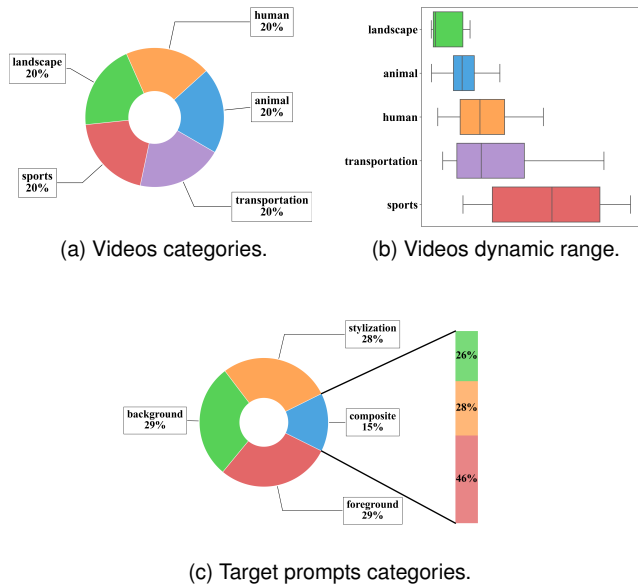


Fig. 10. Statistics of V2VBench videos and prompts.

application scenarios: animals, sports, humans (non-sports), landscapes, and transportation, as shown in Figure 10a.

To maintain compatibility with most methods' configurations, we sample 24 frames from each video clip. The sampling stride is manually adjusted to maintain a balanced dynamic range, ensuring adequate coverage. Figure 10b validates the dynamic range of the preprocessed video clips by measuring the dense optical flow magnitude. The landscape videos exhibit the lowest average dynamic range, while the sports videos demonstrate the highest, aligning with intuition. Additionally, we downscale and crop these video frames to a  $512 \times 512$  spatial resolution, ensuring the

subjects are relatively centered in most frames.

#### 4.1.2 Descriptive and Target Prompts

Apart from the source video input, most methods rely on a descriptive text prompt to outline the source video and a target text prompt to specify desired edits. In V2VBench, we annotate one descriptive text prompt and three target text prompts for each video, organizing 150 editing tasks.

**Descriptive Text Prompts.** We utilize the video captioning approach outlined in SVD [204] to generate descriptive prompts for video clips. First, we employ two caption synthesis models: the image captioning model CoCa [205] annotates the first frame of each video clip, while VideoBLIP [206] provides the video-level caption, effectively capturing spatial and temporal aspects of the video, respectively. Subsequently, these descriptions are integrated using the language model [207] to leverage both visual aspects.

**Target Text Prompts.** To cover the diverse application scenarios of video editing, we create three target text prompts for each video clip featuring different editing types. These include foreground object editing, background editing, and stylization. Inspired by BlanceCC [159], we also incorporate composite edits that combine multiple simple edits, presenting a more challenging task. We manually correct any discrepancies and simplify overly complicated target prompts. As a result, simple edits are almost evenly distributed (approximately 29%) and cover most target prompts, as depicted in Figure 10c. Composite edits, on the other hand, make up 15% of the target prompts.

The curated video-description-editing triplets collectively organize our V2VBench data. For further details about the data curation, please refer to Section A.

## 4.2 Evaluation Metrics

The lack of universally accepted automatic metrics leads existing methods to use diverse evaluation indicators, com-

plicating a comprehensive understanding of their advantages and limitations. Therefore, this survey employs eight evaluation metrics to provide a well-rounded assessment.

**Frames Quality.** Before considering all frames collectively, the quality of each frame constitutes the fundamental basis for determining the overall video quality. We utilize the LAION aesthetic predictor [208], calibrated based on human rankings, to assess the edited video frames. This predictor evaluates subjective aspects including layout, richness, artistry, and visual appeal [115]. Subsequently, we compute the average aesthetic scores to derive the overall quality score of the edited video.

**Video Quality.** Alongside frame-by-frame evaluation, we employ the DOVER score [209] for video-level assessment. DOVER is the state-of-the-art video quality assessment method trained on a large-scale human-ranked video dataset. In addition to aesthetic considerations, the DOVER score evaluates technical aspects including artifacts, distortion, blurring, and meaningfulness.

**Semantic Consistency.** CLIP [198] vision embeddings are widely used to capture image semantic information. The cosine similarity between adjacent frames’ CLIP embeddings is a standard metric for assessing inter-frame consistency and the overall smoothness of the edited video.

**Object Consistency.** Beyond evaluating semantic consistency, we examine whether object-level appearance remains consistent in the edited videos. We employ DINO [210], [211], a self-supervised pre-trained image embedding model, to compute object-level inter-frame similarity.

**Frames Text Alignment.** In addition to assessing the visual quality of the edited videos, alignment with the target text prompts is crucial for controllable video manipulation. CLIP score [198] is the most widely used metric for evaluating vision-text alignment. Following established methods, we compute the CLIP score frame by frame and aggregate the scores by averaging across all frames.

**Video Text Alignment.** Isolated frames are not able to fully represent motion and the original CLIP score may not always capture video-level alignment accurately. We also compute the ViCLIP score [212]. Trained on video-text pairs, the ViCLIP score assesses alignment between spatio-temporal content and target prompts.

**Frames Pick Score.** Human preferences are sometimes complex and cannot be fully captured by feature-level similarity alone. The Pick Score [213] is a CLIP-based scoring function trained on large-scale human preference annotations, considering both image and text inputs to reflect content quality and alignments. We calculate the frame-wise Pick Score and average them as a metric.

**Motion Alignment.** Maintaining consistent motion alignment with the input source video is crucial. To evaluate this, we utilize optical flow computed by GMFlow [118] for each source-editing video pair and measure their difference, also known as endpoint error (EPE). To align with other metrics, which aim for higher values indicating better performance, we negate the final EPE.

**Memory Usage and Running Time.** Besides quality considerations, efficiency metrics such as peak memory usage and running time underscore the strengths and weaknesses of methods. An ideal method should run efficiently on consumer-level devices. Peak memory usage could pose

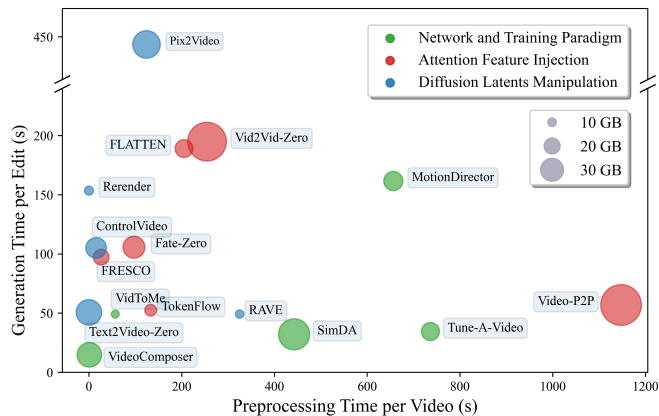


Fig. 11. Memory usage and running time comparison of 16 diffusion model-based video editing methods. The color represents the category, and the radius indicates peak memory usage.

a barrier in broader usage scenarios, making it a crucial efficiency metric to monitor. Running time is categorized into preprocessing time and generation time. Preprocessing for a source video is performed only once and does not need to be repeated for each subsequent editing of the same video. It includes depth map extraction, latent inversion, and sample-specific fine-tuning. Generation time is required for each editing instance, such as diffusion model sampling.

### 4.3 Comparative Analysis

We reimplement 16 methods utilizing their officially released code repositories and weights (if available) on the 50 standardized video clips mentioned in Section 4.1. To ensure a fair and unbiased comparison, we exclude methods that heavily rely on external image editing methods (e.g. LAMP [158] and CCEdit [159]) or require prompts beyond text (e.g. interactive point-based methods). Furthermore, certain methods that demanded excessively prolonged processing times (e.g. LNA-based methods) are also excluded. More implementation details are in Section A.2.

Table 1 presents the quality metrics, Figure 11 presents the efficiency metrics, and Figure 12 provides a visualization of the results for each method, categorized by task.

**No single method exhibits dominance across all metrics.** This emphasizes the necessity to consider various aspects. Fate-Zero [146] demonstrates the best semantic consistency and motion alignment. The methods involving diffusion steps refinement, as described in Section 3.3, excel in the remaining six metrics. Notably, no single method becomes the winner in more than three metrics.

**Feature injection methods exhibit advantages in motion alignment.** For the motion alignment metric, even the third-ranked feature injection method outperforms the best scores from the other categories. When the primary objective is to preserve the source video’s motion while modifying its appearance, feature injection methods are advisable for exploration.

**Efficiency is highly dependent on the methods’ design.** Although feature injection and diffusion latent manipulation methods may slightly increase generation time per edit, they typically require significantly less preprocessing time.



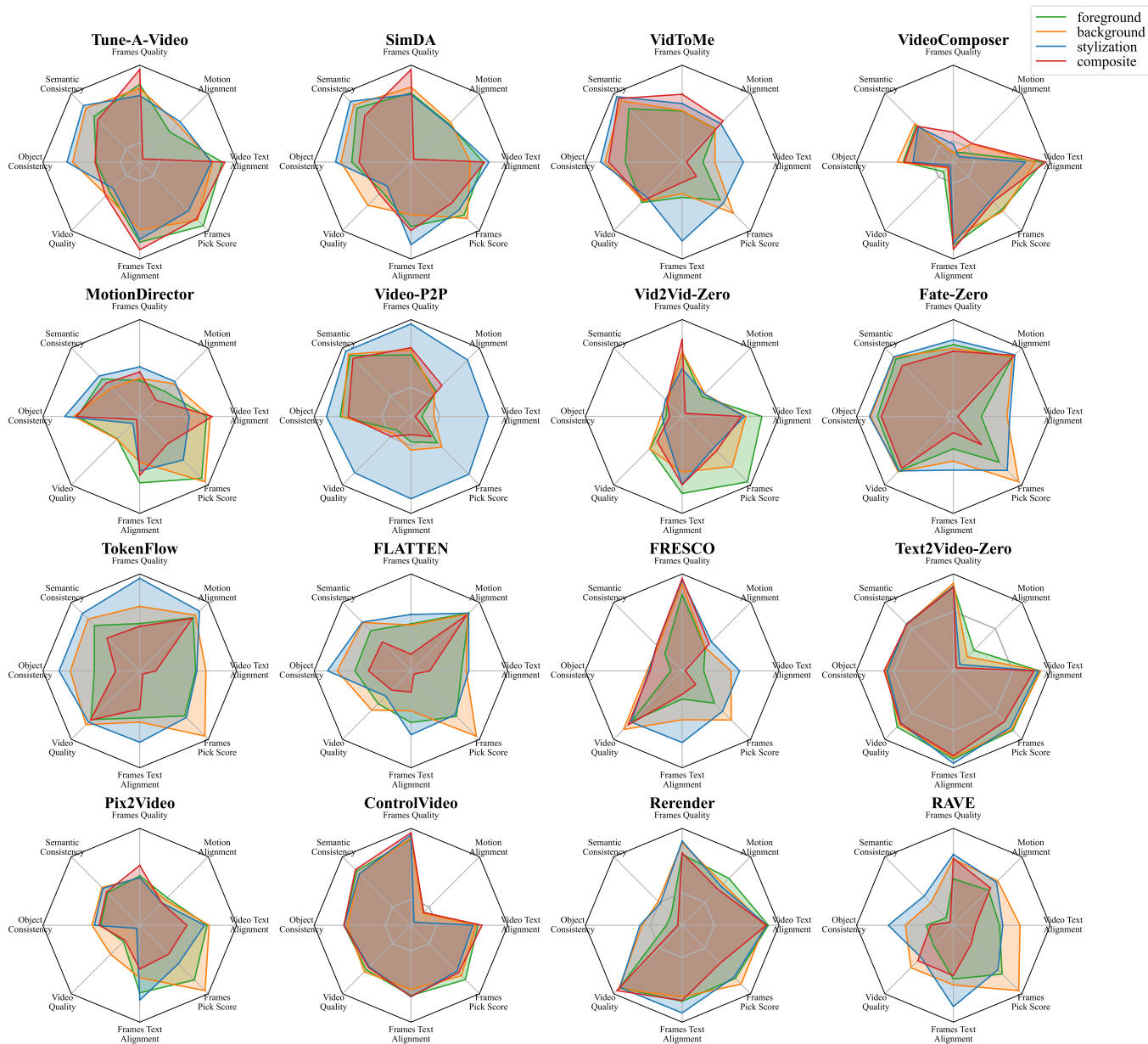


Fig. 12. Further comparisons on V2VBench. Each color represents the metrics for different editing types. Please refer to appendix Section A for additional details and normalization methods.

In contrast, test-time tuning-based methods<sup>†</sup> generally demand substantially higher preprocessing time and memory costs. VidToMe [167], TokenFlow [34], Rerender [138], and RAVE [139] exhibit superiority in running efficiency and are compatible with many consumer-level devices while delivering satisfactory performance on several metrics.

**Certain methods exhibit performance disparities across different tasks.** Figure 12 indicates Tune-A-Video [163] and SimDA [165] demonstrate an evident decline in motion alignment for more challenging composited editing tasks. Video-P2P [144] exhibits greater proficiency in stylization compared to other tasks. Fate-Zero [146] emphasizes frame consistency but exhibits relative weakness in text alignment, particularly for more challenging composited editing tasks. The results of Rerender [138] suggest that it complements the weaknesses of Fate-Zero. Text2Video-Zero [141] and

ControlVideo [137] perform consistently well across all tasks and metrics, except for motion alignment with the source video. Further research should explore ways to maintain high-level performance across different tasks.

## 5 CHALLENGES AND EMERGING TRENDS

Generative methods based on diffusion models have become widely accepted solutions for video editing, with significant advancements achieved in both academic research and commercial applications. Nonetheless, their full potential in video editing remains underexplored. This section outlines unresolved issues and promising opportunities for future exploration.

**Video Data and Foundation Models.** The success of image generation and editing is primarily due to the availability

of large-scale, high-quality image datasets and foundational image models. However, commonly used video datasets are relatively small and low quality [204] because collecting, filtering, and storing video samples are significantly more challenging. Additionally, most available video content is derived from real-world scenarios, offering less fantastical and imaginative content than images. Although new video datasets and foundation models are being developed [212], [214], [215], [216], their performance in generating fantastical and imaginative content is still inferior to image counterparts. An ideal dataset and training protocol for video foundation models may need to integrate data from multiple sources, such as images, videos, 3D, and even 4D content, along with diverse pretext objectives.

**Efficiency.** The inference time for diffusion models is a widely recognized constraint compared to other generative models, such as GANs [168] and VAEs [40], [41], [53], which only require a single forward pass. Accelerating the reverse diffusion process is an active area of research and remains an unsolved challenge [217], [218], [219], [220], [221], [222]. Backbone design also significantly impacts both training and inference efficiency. Despite efforts to design efficient architectures [21], [84], [163], [165], [223], further reducing processing time and memory usage remains a valuable topic for exploration.

**Editing Precision.** A frequent issue with current editing methods is editing spillover: target attributes intended for one object sometimes affect other objects that should remain unmodified. Beyond the text and point prompts discussed in this paper, providing fine-grained spatio-temporal control remains challenging. Developing precise prompting formats that avoid complex interactions is essential for improving control accuracy. Additionally, exploring multimodal prompts offers the potential for greater flexibility.

**Evaluation.** Currently, widely used metrics predominantly rely on image-based models rather than video-based ones. The importance of alignment in video tasks is often overlooked. Moreover, employing multiple metrics for comprehensive coverage can be cumbersome and may not consistently align with human intuition when assessed individually. A unified metric is necessary to simplify comparisons and better capture intuitive assessments.

## 6 CONCLUSION

This paper extensively dives into diffusion model-based video editing methods, providing detailed formulations and explanations of their intrinsic dependencies. It addresses the gap left by previous studies, which often treated video editing as an accessory task with simplistic descriptions. We categorize video editing methods based on their core technologies: network architecture innovation, feature injection, diffusion, video representation, and control signals. Additionally, we outline the evolutionary trajectory of methods within each category. Furthermore, we introduce V2VBench, which comprehensively evaluates 150 edits across 4 editing tasks using 10 metrics. We compare 16 methods on V2VBench to provide comprehensive insights. Finally, we address research challenges and outline promising directions for further exploration.

## APPENDIX A

### IMPLEMENTATION OF V2VBENCH

#### A.1 Prompts Generation

As mentioned in Section 4.1.2, the following prompts are used to refine video descriptions generated by vision-language models:

I need a succinct and accurate video description combining two provided captions. The resulting caption should capture the essence of both captions without excessive adjectives. Aim for clarity and brevity. The two captions are: [video captions]

We generate the target prompts using the following prompts:

I will provide a source video caption, and your task is to provide four types of editing: 1. Foreground: Replace the foreground object in the video with another object. 2. Background: Replace the background object in the video with another object. 3. Stylization: Change the style of the video. 4. Composite: Combine two or more editing types from 1-3. The reference caption is: [source video caption]; Please present the results in the following format: Caption: [edited caption] Type: [editing type]

#### A.2 Experiment Details

All experiments are conducted on a single NVIDIA A100 80GB GPU. All methods use StableDiffusion [5] v1-5<sup>1</sup> as the pre-trained foundation model, except for VideoComposer [161] and MotionDirector [36], which require video-pretrained models. We uniformly use ControlNet [54] v1-1-depth<sup>2</sup> and MiDaS [171] to extract the depth map for methods relying on structural information. The negative prompt "long body, low-res, bad anatomy, bad hands, missing fingers, extra digit, fewer digits, cropped, worst quality, low quality, deformed body, bloated, ugly, blurry, low res, unaesthetic" is used where applicable. All methods run with xFormer [224] enabled to avoid out-of-memory issues. Other configurations adhere to those specified in the original repositories of the respective methods. We follow the code in cases where code configurations differ from those reported in the papers.

## REFERENCES

- [1] J. Sohl-Dickstein, E. A. Weiss, N. Maheswaranathan, and S. Ganguli, "Deep unsupervised learning using nonequilibrium thermodynamics," in *ICML*, vol. 37. JMLR.org, 2015, pp. 2256–2265. 1, 2, 4
- [2] A. Q. Nichol, P. Dhariwal, A. Ramesh, P. Shyam, P. Mishkin, B. McGrew, I. Sutskever, and M. Chen, "GLIDE: towards photorealistic image generation and editing with text-guided diffusion models," in *ICML*, vol. 162. PMLR, 2022, pp. 16784–16804. 1, 3, 4

1. <https://huggingface.co/runwayml/stable-diffusion-v1-5>  
 2. <https://huggingface.co/lllyasviel/ControlNet-v1-1>

- [3] A. Ramesh, P. Dhariwal, A. Nichol, C. Chu, and M. Chen, "Hierarchical text-conditional image generation with CLIP latents," *CoRR*, vol. abs/2204.06125, 2022. **1, 3**
- [4] C. Saharia, W. Chan, S. Saxena, L. Li, J. Whang, E. L. Denton, S. K. S. Ghasemipour, R. G. Lopes, B. K. Ayan, T. Salimans, J. Ho, D. J. Fleet, and M. Norouzi, "Photorealistic text-to-image diffusion models with deep language understanding," in *NeurIPS*, 2022. **1, 3, 4, 5**
- [5] R. Rombach, A. Blattmann, D. Lorenz, P. Esser, and B. Ommer, "High-resolution image synthesis with latent diffusion models," in *CVPR*. IEEE, 2022, pp. 10 674–10 685. **1, 3, 4, 5, 13, 14, 18**
- [6] W. Li, X. Xu, X. Xiao, J. Liu, H. Yang, G. Li, Z. Wang, Z. Feng, Q. She, Y. Lyu, and H. Wu, "Upainting: Unified text-to-image diffusion generation with cross-modal guidance," *CoRR*, vol. abs/2210.16031, 2022. **1, 3**
- [7] Y. Balaji, S. Nah, X. Huang, A. Vahdat, J. Song, K. Kreis, M. Aittala, T. Aila, S. Laine, B. Catanzaro, T. Karras, and M. Liu, "ediff-i: Text-to-image diffusion models with an ensemble of expert denoisers," *CoRR*, vol. abs/2211.01324, 2022. **1, 5**
- [8] Z. Feng, Z. Zhang, X. Yu, Y. Fang, L. Li, X. Chen, Y. Lu, J. Liu, W. Yin, S. Feng, Y. Sun, L. Chen, H. Tian, H. Wu, and H. Wang, "Ernie-vilg 2.0: Improving text-to-image diffusion model with knowledge-enhanced mixture-of-denoising-experts," in *CVPR*. IEEE, 2023, pp. 10 135–10 145. **1**
- [9] G. Kim, T. Kwon, and J. C. Ye, "Diffusionclip: Text-guided diffusion models for robust image manipulation," in *CVPR*. IEEE, 2022, pp. 2416–2425. **1, 4**
- [10] C. Saharia, W. Chan, H. Chang, C. A. Lee, J. Ho, T. Salimans, D. J. Fleet, and M. Norouzi, "Palette: Image-to-image diffusion models," in *SIGGRAPH*. ACM, 2022, pp. 15:1–15:10. **1, 3**
- [11] M. Brack, F. Friedrich, K. Kornmeier, L. Tsaban, P. Schramowski, K. Kersting, and A. Passos, "LEDITS++: limitless image editing using text-to-image models," *CoRR*, vol. abs/2311.16711, 2023. **1**
- [12] B. Kawar, S. Zada, O. Lang, O. Tov, H. Chang, T. Dekel, I. Mosseri, and M. Irani, "Imagic: Text-based real image editing with diffusion models," in *CVPR*. IEEE, 2023, pp. 6007–6017. **1**
- [13] A. Hertz, R. Mokady, R. Tenenbaum, K. Aberman, Y. Pritch, and D. Cohen-Or, "Prompt-to-prompt image editing with cross-attention control," in *ICLR*, 2023. **1, 5, 9, 10**
- [14] N. Tumanyan, M. Geyer, S. Bagon, and T. Dekel, "Plug-and-play diffusion features for text-driven image-to-image translation," in *CVPR*. IEEE, 2023, pp. 1921–1930. **1, 5, 8, 10, 12**
- [15] M. Cao, X. Wang, Z. Qi, Y. Shan, X. Qie, and Y. Zheng, "Masactrl: Tuning-free mutual self-attention control for consistent image synthesis and editing," in *ICCV*. IEEE, 2023, pp. 22 503–22 513. **1, 5, 9, 10, 13**
- [16] T. Brooks, A. Holynski, and A. A. Efros, "Instructpix2pix: Learning to follow image editing instructions," in *CVPR*. IEEE, 2023, pp. 18 392–18 402. **1, 8, 9, 10**
- [17] J. Ho, T. Salimans, A. A. Gritsenko, W. Chan, M. Norouzi, and D. J. Fleet, "Video diffusion models," in *NeurIPS*, 2022. **1, 5**
- [18] J. Ho, W. Chan, C. Saharia, J. Whang, R. Gao, A. A. Gritsenko, D. P. Kingma, B. Poole, M. Norouzi, D. J. Fleet, and T. Salimans, "Imagen video: High definition video generation with diffusion models," *CoRR*, vol. abs/2210.02303, 2022. **1, 5, 9**
- [19] A. Blattmann, R. Rombach, H. Ling, T. Dockhorn, S. W. Kim, S. Fidler, and K. Kreis, "Align your latents: High-resolution video synthesis with latent diffusion models," in *CVPR*. IEEE, 2023, pp. 22 563–22 575. **1, 5**
- [20] Y. Guo, C. Yang, A. Rao, Y. Wang, Y. Qiao, D. Lin, and B. Dai, "Animatediff: Animate your personalized text-to-image diffusion models without specific tuning," *CoRR*, vol. abs/2307.04725, 2023. **1, 5, 6, 8, 9, 13**
- [21] X. Ma, Y. Wang, G. Jia, X. Chen, Z. Liu, Y. Li, C. Chen, and Y. Qiao, "Latte: Latent diffusion transformer for video generation," *CoRR*, vol. abs/2401.03048, 2024. **1, 5, 6, 18**
- [22] R. Girdhar, M. Singh, A. Brown, Q. Duval, S. Azadi, S. S. Rambhatla, A. Shah, X. Yin, D. Parikh, and I. Misra, "Emu video: Factorizing text-to-video generation by explicit image conditioning," *CoRR*, vol. abs/2311.10709, 2023. **1, 6**
- [23] H. Cao, C. Tan, Z. Gao, G. Chen, P. Heng, and S. Z. Li, "A survey on generative diffusion model," *CoRR*, vol. abs/2209.02646, 2022. **1**
- [24] Z. Chang, G. A. Koulouris, and H. P. H. Shum, "On the design fundamentals of diffusion models: A survey," *CoRR*, vol. abs/2306.04542, 2023. **1**
- [25] A. Ulhaq, N. Akhtar, and G. Pogrebna, "Efficient diffusion models for vision: A survey," *CoRR*, vol. abs/2210.09292, 2022. **1**
- [26] L. Yang, Z. Zhang, Y. Song, S. Hong, R. Xu, Y. Zhao, W. Zhang, B. Cui, and M. Yang, "Diffusion models: A comprehensive survey of methods and applications," *ACM Comput. Surv.*, vol. 56, no. 4, pp. 105:1–105:39, 2024. **1**
- [27] C. Zhang, C. Zhang, M. Zhang, and I. S. Kweon, "Text-to-image diffusion models in generative AI: A survey," *CoRR*, vol. abs/2303.07909, 2023. **1**
- [28] T. Zhang, Z. Wang, J. Huang, M. T. Mohiuddin, and W. Shi, "A survey of diffusion based image generation models: Issues and their solutions," *CoRR*, vol. abs/2308.13142, 2023. **1**
- [29] Y. Huang, J. Huang, Y. Liu, M. Yan, J. Lv, J. Liu, W. Xiong, H. Zhang, S. Chen, and L. Cao, "Diffusion model-based image editing: A survey," *CoRR*, vol. abs/2402.17525, 2024. **1, 12**
- [30] R. Po, W. Yifan, V. Golyanik, K. Aberman, J. T. Barron, A. H. Bermanno, E. R. Chan, T. Dekel, A. Holynski, A. Kanazawa, C. K. Liu, L. Liu, B. Mildenhall, M. Nießner, B. Ommer, C. Theobalt, P. Wonka, and G. Wetzstein, "State of the art on diffusion models for visual computing," *CoRR*, vol. abs/2310.07204, 2023. **1**
- [31] J. Liu, X. Huang, T. Huang, L. Chen, Y. Hou, S. Tang, Z. Liu, W. Ouyang, W. Zuo, J. Jiang, and X. Liu, "A comprehensive survey on 3d content generation," *CoRR*, vol. abs/2402.01166, 2024. **1**
- [32] Z. Xing, Q. Feng, H. Chen, Q. Dai, H. Hu, H. Xu, Z. Wu, and Y. Jiang, "A survey on video diffusion models," *CoRR*, vol. abs/2310.10647, 2023. **1**
- [33] Y. Cong, M. Xu, C. Simon, S. Chen, J. Ren, Y. Xie, J. Pérez-Rúa, B. Rosenhahn, T. Xiang, and S. He, "FLATTEN: optical flow-guided attention for consistent text-to-video editing," *CoRR*, vol. abs/2310.05922, 2023. **2, 7, 10, 15**
- [34] M. Geyer, O. Bar-Tal, S. Bagon, and T. Dekel, "Tokenflow: Consistent diffusion features for consistent video editing," *CoRR*, vol. abs/2307.10373, 2023. **2, 7, 10, 15, 17**
- [35] D. Ceylan, C. P. Huang, and N. J. Mitra, "Pix2video: Video editing using image diffusion," in *ICCV*. IEEE, 2023, pp. 23 149–23 160. **2, 7, 11, 15**
- [36] R. Zhao, Y. Gu, J. Z. Wu, D. J. Zhang, J. Liu, W. Wu, J. Keppo, and M. Z. Shou, "Motiondirector: Motion customization of text-to-video diffusion models," *CoRR*, vol. abs/2310.08465, 2023. **2, 7, 9, 15, 18**
- [37] Y. Gu, Y. Zhou, B. Wu, L. Yu, J. Liu, R. Zhao, J. Z. Wu, D. J. Zhang, M. Z. Shou, and K. Tang, "Videoswap: Customized video subject swapping with interactive semantic point correspondence," *CoRR*, vol. abs/2312.02087, 2023. **2, 7, 14**
- [38] Z. Xu, J. Zhang, J. H. Liew, H. Yan, J. Liu, C. Zhang, J. Feng, and M. Z. Shou, "Magicanimate: Temporally consistent human image animation using diffusion model," *CoRR*, vol. abs/2311.16498, 2023. **2, 7, 14**
- [39] J. Ho, A. Jain, and P. Abbeel, "Denoising diffusion probabilistic models," in *NeurIPS*, 2020. **2, 3, 4, 10**
- [40] D. P. Kingma and M. Welling, "Auto-encoding variational bayes," in *ICLR*, 2014. **2, 3, 14, 18**
- [41] A. van den Oord, O. Vinyals, and K. Kavukcuoglu, "Neural discrete representation learning," in *NIPS*, 2017, pp. 6306–6315. **2, 3, 18**
- [42] D. J. Rezende and S. Mohamed, "Variational inference with normalizing flows," in *ICML*, vol. 37. JMLR.org, 2015, pp. 1530–1538. **2**
- [43] Y. Song, J. Sohl-Dickstein, D. P. Kingma, A. Kumar, S. Ermon, and B. Poole, "Score-based generative modeling through stochastic differential equations," in *ICLR*, 2021. **2, 3, 4**
- [44] A. Hyvärinen, "Estimation of non-normalized statistical models by score matching," *JMLR*, vol. 6, pp. 695–709, 2005. **2**
- [45] Y. Song and S. Ermon, "Generative modeling by estimating gradients of the data distribution," in *NeurIPS*, 2019, pp. 11 895–11 907. **3, 4**
- [46] J. Song, C. Meng, and S. Ermon, "Denoising diffusion implicit models," in *ICLR*, 2021. **3, 4, 7, 8, 11, 13**
- [47] A. Q. Nichol and P. Dhariwal, "Improved denoising diffusion probabilistic models," in *ICML*, vol. 139. PMLR, 2021, pp. 8162–8171. **3, 4**
- [48] P. Dhariwal and A. Q. Nichol, "Diffusion models beat gans on image synthesis," in *NeurIPS*, 2021, pp. 8780–8794. **3, 4**
- [49] J. Ho and T. Salimans, "Classifier-free diffusion guidance," *CoRR*, vol. abs/2207.12598, 2022. **3, 4, 10**

- [50] T. Karras, M. Aittala, T. Aila, and S. Laine, "Elucidating the design space of diffusion-based generative models," in *NeurIPS*, 2022. 3, 4, 11
- [51] J. Ho, C. Saharia, W. Chan, D. J. Fleet, M. Norouzi, and T. Salimans, "Cascaded diffusion models for high fidelity image generation," *J. Mach. Learn. Res.*, vol. 23, pp. 47:1–47:33, 2022. 3
- [52] S. Gu, D. Chen, J. Bao, F. Wen, B. Zhang, D. Chen, L. Yuan, and B. Guo, "Vector quantized diffusion model for text-to-image synthesis," in *CVPR*. IEEE, 2022, pp. 10686–10696. 3
- [53] P. Esser, R. Rombach, and B. Ommer, "Taming transformers for high-resolution image synthesis," in *CVPR*. IEEE, 2021, pp. 12873–12883. 3, 18
- [54] L. Zhang, A. Rao, and M. Agrawala, "Adding conditional control to text-to-image diffusion models," in *ICCV*. IEEE, 2023, pp. 3813–3824. 3, 8, 9, 11, 12, 13, 14, 18
- [55] C. Mou, X. Wang, L. Xie, Y. Wu, J. Zhang, Z. Qi, and Y. Shan, "T2i-adapter: Learning adapters to dig out more controllable ability for text-to-image diffusion models," in *AAAI*. AAAI Press, 2024, pp. 4296–4304. 3, 8, 14
- [56] E. Perez, F. Strub, H. de Vries, V. Dumoulin, and A. C. Courville, "Film: Visual reasoning with a general conditioning layer," in *AAAI*. AAAI Press, 2018, pp. 3942–3951. 4
- [57] Y. Wu and K. He, "Group normalization," in *ECCV (13)*, vol. 11217. Springer, 2018, pp. 3–19. 4
- [58] D. Ulyanov, A. Vedaldi, and V. S. Lempitsky, "Instance normalization: The missing ingredient for fast stylization," *CoRR*, vol. abs/1607.08022, 2016. 4
- [59] X. Huang and S. J. Belongie, "Arbitrary style transfer in real-time with adaptive instance normalization," in *ICCV*. IEEE Computer Society, 2017, pp. 1510–1519. 4
- [60] A. Vaswani, N. Shazeer, N. Parmar, J. Uszkoreit, L. Jones, A. N. Gomez, L. Kaiser, and I. Polosukhin, "Attention is all you need," in *NIPS*, 2017, pp. 5998–6008. 4
- [61] C. Meng, Y. He, Y. Song, J. Song, J. Wu, J. Zhu, and S. Ermon, "Sdedit: Guided image synthesis and editing with stochastic differential equations," in *ICLR*. OpenReview.net, 2022. 4, 9, 12, 13
- [62] R. Mokady, A. Hertz, K. Aberman, Y. Pritch, and D. Cohen-Or, "Null-text inversion for editing real images using guided diffusion models," in *CVPR*. IEEE, 2023, pp. 6038–6047. 4, 9, 10, 11
- [63] L. Tang, M. Jia, Q. Wang, C. P. Phoo, and B. Hariharan, "Emergent correspondence from image diffusion," in *NeurIPS*, 2023. 5, 9, 13, 14
- [64] O. Avrahami, O. Fried, and D. Lischinski, "Blended latent diffusion," *ACM Trans. Graph.*, vol. 42, no. 4, pp. 149:1–149:11, 2023. 5, 10
- [65] O. Avrahami, D. Lischinski, and O. Fried, "Blended diffusion for text-driven editing of natural images," in *CVPR*. IEEE, 2022, pp. 18187–18197. 5, 10
- [66] R. Gal, Y. Alaluf, Y. Atzmon, O. Patashnik, A. H. Bermano, G. Chechik, and D. Cohen-Or, "An image is worth one word: Personalizing text-to-image generation using textual inversion," in *ICLR*, 2023. 5, 9
- [67] N. Ruiz, Y. Li, V. Jampani, Y. Pritch, M. Rubinstein, and K. Aberman, "Dreambooth: Fine tuning text-to-image diffusion models for subject-driven generation," in *CVPR*. IEEE, 2023, pp. 22500–22510. 5, 9
- [68] N. Kumari, B. Zhang, R. Zhang, E. Shechtman, and J. Zhu, "Multi-concept customization of text-to-image diffusion," in *CVPR*. IEEE, 2023, pp. 1931–1941. 5
- [69] Y. Wei, Y. Zhang, Z. Ji, J. Bai, L. Zhang, and W. Zuo, "ELITE: encoding visual concepts into textual embeddings for customized text-to-image generation," in *ICCV*. IEEE, 2023, pp. 15897–15907. 5
- [70] W. Chen, H. Hu, Y. Li, N. Ruiz, X. Jia, M. Chang, and W. W. Cohen, "Subject-driven text-to-image generation via apprenticeship learning," in *NeurIPS*, 2023. 5
- [71] J. Shi, W. Xiong, Z. Lin, and H. J. Jung, "Instantbooth: Personalized text-to-image generation without test-time finetuning," *CoRR*, vol. abs/2304.03411, 2023. 5
- [72] H. Chen, Y. Zhang, X. Wang, X. Duan, Y. Zhou, and W. Zhu, "Disenbooth: Identity-preserving disentangled tuning for subject-driven text-to-image generation," *CoRR*, vol. abs/2305.03374, 2023. 5
- [73] J. Gu, Y. Wang, N. Zhao, T. Fu, W. Xiong, Q. Liu, Z. Zhang, H. Zhang, J. Zhang, H. Jung, and X. E. Wang, "PHOTOSWAP: personalized subject swapping in images," in *NeurIPS*, 2023. 5
- [74] W. Yan, A. Brown, P. Abbeel, R. Girdhar, and S. Azadi, "Motion-conditioned image animation for video editing," *CoRR*, vol. abs/2311.18827, 2023. 5, 7, 8
- [75] E. J. Hu, Y. Shen, P. Wallis, Z. Allen-Zhu, Y. Li, S. Wang, L. Wang, and W. Chen, "Lora: Low-rank adaptation of large language models," in *ICLR*, 2022. 5, 9, 13
- [76] D. Bolya, C. Fu, X. Dai, P. Zhang, C. Feichtenhofer, and J. Hoffman, "Token merging: Your vit but faster," in *ICLR*, 2023. 5, 8
- [77] D. Bolya and J. Hoffman, "Token merging for fast stable diffusion," in *CVPR Workshops*. IEEE, 2023, pp. 4599–4603. 5, 8
- [78] A. Dosovitskiy, L. Beyer, A. Kolesnikov, D. Weissenborn, X. Zhai, T. Unterthiner, M. Dehghani, M. Minderer, G. Heigold, S. Gelly, J. Uszkoreit, and N. Houlsby, "An image is worth 16x16 words: Transformers for image recognition at scale," in *ICLR*, 2021. 5
- [79] U. Singer, A. Polyak, T. Hayes, X. Yin, J. An, S. Zhang, Q. Hu, H. Yang, O. Ashual, O. Gafni, D. Parikh, S. Gupta, and Y. Taigman, "Make-a-video: Text-to-video generation without text-video data," in *ICLR*, 2023. 5
- [80] J. Wang, H. Yuan, D. Chen, Y. Zhang, X. Wang, and S. Zhang, "Modelscope text-to-video technical report," *CoRR*, vol. abs/2308.06571, 2023. 5, 6, 9
- [81] D. J. Zhang, J. Z. Wu, J. Liu, R. Zhao, L. Ran, Y. Gu, D. Gao, and M. Z. Shou, "Show-1: Marrying pixel and latent diffusion models for text-to-video generation," *CoRR*, vol. abs/2309.15818, 2023. 5, 6
- [82] H. Chen, M. Xia, Y. He, Y. Zhang, X. Cun, S. Yang, J. Xing, Y. Liu, Q. Chen, X. Wang, C. Weng, and Y. Shan, "Videocrafter1: Open diffusion models for high-quality video generation," *CoRR*, vol. abs/2310.19512, 2023. 5, 6
- [83] Y. Wang, X. Chen, X. Ma, S. Zhou, Z. Huang, Y. Wang, C. Yang, Y. He, J. Yu, P. Yang, Y. Guo, T. Wu, C. Si, Y. Jiang, C. Chen, C. C. Loy, B. Dai, D. Lin, Y. Qiao, and Z. Liu, "LAVIE: high-quality video generation with cascaded latent diffusion models," *CoRR*, vol. abs/2309.15103, 2023. 5, 6, 10
- [84] S. Chen, M. Xu, J. Ren, Y. Cong, S. He, Y. Xie, A. Sinha, P. Luo, T. Xiang, and J. Pérez-Rúa, "Gentron: Delving deep into diffusion transformers for image and video generation," *CoRR*, vol. abs/2312.04557, 2023. 5, 6, 18
- [85] C. Vondrick, H. Pirsiavash, and A. Torralba, "Generating videos with scene dynamics," in *NIPS*, 2016, pp. 613–621. 5
- [86] M. Saito, E. Matsumoto, and S. Saito, "Temporal generative adversarial nets with singular value clipping," in *ICCV*. IEEE Computer Society, 2017, pp. 2849–2858. 5
- [87] S. Tulyakov, M. Liu, X. Yang, and J. Kautz, "Mocogan: Decomposing motion and content for video generation," in *CVPR*. IEEE, 2018, pp. 1526–1535. 5
- [88] M. Saito, S. Saito, M. Koyama, and S. Kobayashi, "Train sparsely, generate densely: Memory-efficient unsupervised training of high-resolution temporal GAN," *Int. J. Comput. Vis.*, vol. 128, no. 10, pp. 2586–2606, 2020. 5
- [89] C. Wu, L. Huang, Q. Zhang, B. Li, L. Ji, F. Yang, G. Sapiro, and N. Duan, "GODIVA: generating open-domain videos from natural descriptions," *CoRR*, vol. abs/2104.14806, 2021. 5
- [90] I. Skorokhodov, S. Tulyakov, and M. Elhoseiny, "Stylegan-v: A continuous video generator with the price, image quality and perks of stylegan2," in *CVPR*. IEEE, 2022, pp. 3616–3626. 5
- [91] V. Voleti, A. Jolicœur-Martineau, and C. Pal, "MCVD - masked conditional video diffusion for prediction, generation, and interpolation," in *NeurIPS*, 2022. 5
- [92] B. K. P. Horn and B. G. Schunck, "Determining optical flow," *Artif. Intell.*, vol. 17, no. 1-3, pp. 185–203, 1981. 5, 6
- [93] P. Sand and S. J. Teller, "Particle video: Long-range motion estimation using point trajectories," in *CVPR (2)*. IEEE Computer Society, 2006, pp. 2195–2202. 5, 6
- [94] P. Esser, J. Chiu, P. Atighehchian, J. Granskog, and A. Germanidis, "Structure and content-guided video synthesis with diffusion models," in *ICCV*. IEEE, 2023, pp. 7312–7322. 5, 7, 8
- [95] H. Chen, Y. Zhang, X. Cun, M. Xia, X. Wang, C. Weng, and Y. Shan, "Videocrafter2: Overcoming data limitations for high-quality video diffusion models," *CoRR*, vol. abs/2401.09047, 2024. 6
- [96] J. An, S. Zhang, H. Yang, S. Gupta, J. Huang, J. Luo, and X. Yin, "Latent-shift: Latent diffusion with temporal shift for efficient text-to-video generation," *CoRR*, vol. abs/2304.08477, 2023. 6, 8

- [97] X. Chen, Y. Wang, L. Zhang, S. Zhuang, X. Ma, J. Yu, Y. Wang, D. Lin, Y. Qiao, and Z. Liu, "SEINE: short-to-long video diffusion model for generative transition and prediction," *CoRR*, vol. abs/2310.20700, 2023. [6](#), [10](#)
- [98] S. Zhang, J. Wang, Y. Zhang, K. Zhao, H. Yuan, Z. Qin, X. Wang, D. Zhao, and J. Zhou, "I2vgen-xl: High-quality image-to-video synthesis via cascaded diffusion models," *CoRR*, vol. abs/2311.04145, 2023. [6](#), [10](#)
- [99] Z. Li, R. Tucker, N. Snavely, and A. Holynski, "Generative image dynamics," *CoRR*, vol. abs/2309.07906, 2023. [6](#)
- [100] H. Ni, C. Shi, K. Li, S. X. Huang, and M. R. Min, "Conditional image-to-video generation with latent flow diffusion models," in *CVPR*. IEEE, 2023, pp. 18 444–18 455. [6](#)
- [101] W. Ren, H. Yang, G. Zhang, C. Wei, X. Du, S. Huang, and W. Chen, "Consisti2v: Enhancing visual consistency for image-to-video generation," *CoRR*, vol. abs/2402.04324, 2024. [6](#), [10](#)
- [102] X. Gu, C. Wen, J. Song, and Y. Gao, "Seer: Language instructed video prediction with latent diffusion models," *CoRR*, vol. abs/2303.14897, 2023. [6](#)
- [103] W. Harvey, S. Naderiparizi, V. Masrani, C. Weilbach, and F. Wood, "Flexible diffusion modeling of long videos," in *NeurIPS*, 2022. [6](#)
- [104] V. Liu, T. Long, N. Raw, and L. B. Chilton, "Generative disco: Text-to-video generation for music visualization," *CoRR*, vol. abs/2304.08551, 2023. [6](#)
- [105] S. Lee, C. Kong, D. Jeon, and N. Kwak, "Aadiff: Audio-aligned video synthesis with text-to-image diffusion," *CoRR*, vol. abs/2305.04001, 2023. [6](#)
- [106] Y. Jeong, W. Ryoo, S. Lee, D. Seo, W. Byeon, S. Kim, and J. Kim, "The power of sound (tpos): Audio reactive video generation with stable diffusion," in *ICCV*. IEEE, 2023, pp. 7788–7798. [6](#)
- [107] J. Xing, M. Xia, Y. Liu, Y. Zhang, Y. Zhang, Y. He, H. Liu, H. Chen, X. Cun, X. Wang, Y. Shan, and T. Wong, "Make-your-video: Customized video generation using textual and structural guidance," *CoRR*, vol. abs/2306.00943, 2023. [6](#)
- [108] T. Chen, C. H. Lin, H. Tseng, T. Lin, and M. Yang, "Motion-conditioned diffusion model for controllable video synthesis," *CoRR*, vol. abs/2304.14404, 2023. [6](#)
- [109] Z. Chen, J. Qing, and J. H. Zhou, "Cinematic mindscapes: High-quality video reconstruction from brain activity," in *NeurIPS*, 2023. [6](#)
- [110] J. Zhu, H. Yang, H. He, W. Wang, Z. Tuo, W. Cheng, L. Gao, J. Song, and J. Fu, "Moviefactory: Automatic movie creation from text using large generative models for language and images," in *ACM Multimedia*. ACM, 2023, pp. 9313–9319. [6](#)
- [111] Z. Tang, Z. Yang, C. Zhu, M. Zeng, and M. Bansal, "Any-to-any generation via composable diffusion," in *NeurIPS*, 2023. [6](#)
- [112] S. Wu, H. Fei, L. Qu, W. Ji, and T. Chua, "Next-gpt: Any-to-any multimodal LLM," *CoRR*, vol. abs/2309.05519, 2023. [6](#)
- [113] A. W. Harley, Z. Fang, and K. Fragkiadaki, "Particle video revisited: Tracking through occlusions using point trajectories," in *ECCV*, vol. 13682. Springer, 2022, pp. 59–75. [6](#)
- [114] V. K. M. Vadakital, A. Dziembowski, G. Lafruit, F. Thudor, G. Lee, and P. Rondao-Alfaca, "The MPEG immersive video standard - current status and future outlook," *IEEE Multim.*, vol. 29, no. 3, pp. 101–111, 2022. [6](#), [8](#)
- [115] Z. Huang, Y. He, J. Yu, F. Zhang, C. Si, Y. Jiang, Y. Zhang, T. Wu, Q. Jin, N. Chanpaisit, Y. Wang, X. Chen, L. Wang, D. Lin, Y. Qiao, and Z. Liu, "Vbench: Comprehensive benchmark suite for video generative models," *CoRR*, vol. abs/2311.17982, 2023. [6](#), [14](#), [16](#)
- [116] Y. Liu, X. Cun, X. Liu, X. Wang, Y. Zhang, H. Chen, Y. Liu, T. Zeng, R. H. Chan, and Y. Shan, "Evalcrafter: Benchmarking and evaluating large video generation models," *CoRR*, vol. abs/2310.11440, 2023. [6](#), [14](#)
- [117] Z. Teed and J. Deng, "RAFT: recurrent all-pairs field transforms for optical flow," in *ECCV*, vol. 12347. Springer, 2020, pp. 402–419. [6](#), [8](#), [12](#)
- [118] H. Xu, J. Zhang, J. Cai, H. Rezatofighi, and D. Tao, "Gmflow: Learning optical flow via global matching," in *CVPR*. IEEE, 2022, pp. 8111–8120. [6](#), [16](#)
- [119] A. Dosovitskiy, P. Fischer, E. Ilg, P. Häusser, C. Hazirbas, V. Golkov, P. van der Smagt, D. Cremers, and T. Brox, "Flownet: Learning optical flow with convolutional networks," in *ICCV*. IEEE Computer Society, 2015, pp. 2758–2766. [6](#)
- [120] N. Mayer, E. Ilg, P. Häusser, P. Fischer, D. Cremers, A. Dosovitskiy, and T. Brox, "A large dataset to train convolutional networks for disparity, optical flow, and scene flow estimation," in *CVPR*. IEEE Computer Society, 2016, pp. 4040–4048. [6](#)
- [121] D. J. Butler, J. Wulff, G. B. Stanley, and M. J. Black, "A naturalistic open source movie for optical flow evaluation," in *ECCV*, vol. 7577. Springer, 2012, pp. 611–625. [6](#)
- [122] A. Gaidon, Q. Wang, Y. Cabon, and E. Vig, "Virtual worlds as proxy for multi-object tracking analysis," *CoRR*, vol. abs/1605.06457, 2016. [6](#)
- [123] Y. Ma, Y. He, X. Cun, X. Wang, S. Chen, X. Li, and Q. Chen, "Follow your pose: Pose-guided text-to-video generation using pose-free videos," in *AAAI*. AAAI Press, 2024, pp. 4117–4125. [7](#), [14](#)
- [124] J. Karras, A. Holynski, T. Wang, and I. Kemelmacher-Shlizerman, "Dreampose: Fashion image-to-video synthesis via stable diffusion," in *ICCV*. IEEE, 2023, pp. 22 623–22 633. [7](#), [14](#)
- [125] T. Wang, L. Li, K. Lin, Y. Zhai, C.-C. Lin, Z. Yang, H. Zhang, Z. Liu, and L. Wang, "Disco: Disentangled control for realistic human dance generation," *CoRR*, vol. abs/2307.00040, 2023. [7](#), [14](#)
- [126] S. Tu, Q. Dai, Z. Cheng, H. Hu, X. Han, Z. Wu, and Y. Jiang, "Motioneditor: Editing video motion via content-aware diffusion," *CoRR*, vol. abs/2311.18830, 2023. [7](#), [14](#)
- [127] D. Chang, Y. Shi, Q. Gao, J. Fu, H. Xu, G. Song, Q. Yan, Y. Zhu, X. Yang, and M. Soleymani, "Magicpose: Realistic human poses and facial expressions retargeting with identity-aware diffusion," *CoRR*, vol. abs/2311.12052, 2024. [7](#), [14](#)
- [128] L. Hu, X. Gao, P. Zhang, K. Sun, B. Zhang, and L. Bo, "Animate anyone: Consistent and controllable image-to-video synthesis for character animation," *CoRR*, vol. abs/2311.17117, 2023. [7](#), [14](#)
- [129] Y. Deng, R. Wang, Y. Zhang, Y. Tai, and C. Tang, "Dragvideo: Interactive drag-style video editing," *CoRR*, vol. abs/2312.02216, 2023. [7](#), [13](#)
- [130] Y. Teng, E. Xie, Y. Wu, H. Han, Z. Li, and X. Liu, "Drag-a-video: Non-rigid video editing with point-based interaction," *CoRR*, vol. abs/2312.02936, 2023. [7](#), [13](#)
- [131] W. Chai, X. Guo, G. Wang, and Y. Lu, "Stablevideo: Text-driven consistency-aware diffusion video editing," in *ICCV*. IEEE, 2023, pp. 22 983–22 993. [7](#), [13](#)
- [132] Y. Lee, J. G. Jang, Y. Chen, E. Qiu, and J. Huang, "Shape-aware text-driven layered video editing," in *CVPR*. IEEE, 2023, pp. 14 317–14 326. [7](#), [13](#)
- [133] P. Couairon, C. Rambour, J. Haugeard, and N. Thome, "Videdit: Zero-shot and spatially aware text-driven video editing," *CoRR*, vol. abs/2306.08707, 2023. [7](#), [12](#)
- [134] S. Chang, H. Chen, and T. Liu, "Diffusionatlas: High-fidelity consistent diffusion video editing," *CoRR*, vol. abs/2312.03772, 2023. [7](#), [13](#)
- [135] Y. Kasten, D. Ofri, O. Wang, and T. Dekel, "Layered neural atlases for consistent video editing," *ACM Trans. Graph.*, vol. 40, no. 6, pp. 210:1–210:12, 2021. [7](#), [12](#), [14](#)
- [136] H. Ouyang, Q. Wang, Y. Xiao, Q. Bai, J. Zhang, K. Zheng, X. Zhou, Q. Chen, and Y. Shen, "Codef: Content deformation fields for temporally consistent video processing," *CoRR*, vol. abs/2308.07926, 2023. [7](#), [12](#)
- [137] Y. Zhang, Y. Wei, D. Jiang, X. Zhang, W. Zuo, and Q. Tian, "Controlvideo: Training-free controllable text-to-video generation," *CoRR*, vol. abs/2305.13077, 2023. [7](#), [11](#), [15](#), [17](#)
- [138] S. Yang, Y. Zhou, Z. Liu, and C. C. Loy, "Rerender A video: Zero-shot text-guided video-to-video translation," in *SIGGRAPH*. ACM, 2023, pp. 95:1–95:11. [7](#), [11](#), [15](#), [17](#)
- [139] O. Kara, B. Kurtkaya, H. Yesiltepe, J. M. Rehg, and P. Yanardag, "RAVE: randomized noise shuffling for fast and consistent video editing with diffusion models," *CoRR*, vol. abs/2312.04524, 2023. [7](#), [12](#), [15](#), [17](#)
- [140] W. Chen, J. Wu, P. Xie, H. Wu, J. Li, X. Xia, X. Xiao, and L. Lin, "Control-a-video: Controllable text-to-video generation with diffusion models," *CoRR*, vol. abs/2305.13840, 2023. [7](#), [11](#)
- [141] L. Khachatryan, A. Movsisyan, V. Tadevosyan, R. Henschel, Z. Wang, S. Navasardyan, and H. Shi, "Text2video-zero: Text-to-image diffusion models are zero-shot video generators," in *ICCV*. IEEE, 2023, pp. 15 908–15 918. [7](#), [11](#), [15](#), [17](#)
- [142] E. Chu, S. Lin, and J. Chen, "Video controlnet: Towards temporally consistent synthetic-to-real video translation using conditional image diffusion models," *CoRR*, vol. abs/2305.19193, 2023. [7](#), [11](#)
- [143] S. Yang, Y. Zhou, Z. Liu, and C. C. Loy, "FRESCO: spatial-temporal correspondence for zero-shot video translation," *CoRR*, vol. abs/2403.12962, 2024. [7](#), [10](#), [15](#)
- [144] S. Liu, Y. Zhang, W. Li, Z. Lin, and J. Jia, "Video-p2p: Video editing with cross-attention control," 2023. [7](#), [9](#), [15](#), [17](#)

- [145] W. Wang, K. Xie, Z. Liu, H. Chen, Y. Cao, X. Wang, and C. Shen, "Zero-shot video editing using off-the-shelf image diffusion models," *CoRR*, vol. abs/2303.17599, 2023. [7](#), [9](#), [15](#)
- [146] C. Qi, X. Cun, Y. Zhang, C. Lei, X. Wang, Y. Shan, and Q. Chen, "Fatezero: Fusing attentions for zero-shot text-based video editing," in *ICCV*. IEEE, 2023, pp. 15886–15896. [7](#), [10](#), [15](#), [16](#), [17](#)
- [147] C. Shin, H. Kim, C. H. Lee, S. Lee, and S. Yoon, "Edit-a-video: Single video editing with object-aware consistency," in *ACML*, vol. 222. PMLR, 2023, pp. 1215–1230. [7](#), [10](#)
- [148] Y. Zhao, E. Xie, L. Hong, Z. Li, and G. H. Lee, "Make-a-protagonist: Generic video editing with an ensemble of experts," *CoRR*, vol. abs/2305.08850, 2023. [7](#), [10](#)
- [149] J. Bai, T. He, Y. Wang, J. Guo, H. Hu, Z. Liu, and J. Bian, "Unedit: A unified tuning-free framework for video motion and appearance editing," *CoRR*, vol. abs/2402.13185, 2024. [7](#), [9](#), [10](#)
- [150] M. Ku, C. Wei, W. Ren, H. Yang, and W. Chen, "Anyv2v: A plug-and-play framework for any video-to-video editing tasks," *CoRR*, vol. abs/2403.14468, 2024. [7](#), [9](#), [10](#)
- [151] H. Jeong, G. Y. Park, and J. C. Ye, "VMC: video motion customization using temporal attention adaption for text-to-video diffusion models," *CoRR*, vol. abs/2312.00845, 2023. [7](#), [9](#)
- [152] E. Molad, E. Horwitz, D. Valevski, A. Rav-Acha, Y. Matias, Y. Prithvi, Y. Leviathan, and Y. Hoshen, "Dreamix: Video diffusion models are general video editors," *CoRR*, vol. abs/2302.01329, 2023. [7](#), [9](#)
- [153] Y. Song, W. Shin, J. Lee, J. Kim, and N. Kwak, "SAVE: protagonist diversification with structure agnostic video editing," *CoRR*, vol. abs/2312.02503, 2023. [7](#), [9](#)
- [154] B. Qin, J. Li, S. Tang, T. Chua, and Y. Zhuang, "Instructvid2vid: Controllable video editing with natural language instructions," *CoRR*, vol. abs/2305.12328, 2023. [7](#), [9](#)
- [155] J. Cheng, T. Xiao, and T. He, "Consistent video-to-video transfer using synthetic dataset," *CoRR*, vol. abs/2311.00213, 2023. [7](#)
- [156] J. H. Liew, H. Yan, J. Zhang, Z. Xu, and J. Feng, "Magicedit: High-fidelity and temporally coherent video editing," *CoRR*, vol. abs/2308.14749, 2023. [7](#), [8](#)
- [157] H. Jeong and J. C. Ye, "Ground-a-video: Zero-shot grounded video editing using text-to-image diffusion models," *CoRR*, vol. abs/2310.01107, 2023. [7](#), [8](#), [11](#)
- [158] R. Wu, L. Chen, T. Yang, C. Guo, C. Li, and X. Zhang, "LAMP: learn a motion pattern for few-shot-based video generation," *CoRR*, vol. abs/2310.10769, 2023. [7](#), [8](#), [11](#), [16](#)
- [159] R. Feng, W. Weng, Y. Wang, Y. Yuan, J. Bao, C. Luo, Z. Chen, and B. Guo, "Ccedit: Creative and controllable video editing via diffusion models," *CoRR*, vol. abs/2309.16496, 2023. [7](#), [8](#), [11](#), [14](#), [15](#), [16](#)
- [160] F. Liang, B. Wu, J. Wang, L. Yu, K. Li, Y. Zhao, I. Misra, J. Huang, P. Zhang, P. Vajda, and D. Marculescu, "Flowvid: Taming imperfect optical flows for consistent video-to-video synthesis," *CoRR*, vol. abs/2312.17681, 2023. [7](#), [8](#)
- [161] X. Wang, H. Yuan, S. Zhang, D. Chen, J. Wang, Y. Zhang, Y. Shen, D. Zhao, and J. Zhou, "Videocomposer: Compositional video synthesis with motion controllability," in *NeurIPS*, 2023. [7](#), [8](#), [15](#), [18](#)
- [162] Z. Hu and D. Xu, "Videocontrolnet: A motion-guided video-to-video translation framework by using diffusion model with controlnet," *CoRR*, vol. abs/2307.14073, 2023. [7](#), [8](#)
- [163] J. Z. Wu, Y. Ge, X. Wang, S. W. Lei, Y. Gu, Y. Shi, W. Hsu, Y. Shan, X. Qie, and M. Z. Shou, "Tune-a-video: One-shot tuning of image diffusion models for text-to-video generation," in *ICCV*. IEEE, 2023, pp. 7589–7599. [6](#), [7](#), [9](#), [10](#), [14](#), [15](#), [17](#), [18](#)
- [164] Z. Zhang, B. Li, X. Nie, C. Han, T. Guo, and L. Liu, "Towards consistent video editing with text-to-image diffusion models," in *NeurIPS*, 2023. [7](#), [9](#)
- [165] Z. Xing, Q. Dai, H. Hu, Z. Wu, and Y. Jiang, "Simda: Simple diffusion adapter for efficient video generation," *CoRR*, vol. abs/2308.09710, 2023. [7](#), [15](#), [17](#), [18](#)
- [166] B. Wu, C. Chuang, X. Wang, Y. Jia, K. Krishnakumar, T. Xiao, F. Liang, L. Yu, and P. Vajda, "Fairy: Fast parallelized instruction-guided video-to-video synthesis," *CoRR*, vol. abs/2312.13834, 2023. [7](#), [8](#)
- [167] X. Li, C. Ma, X. Yang, and M. Yang, "Vidtope: Video token merging for zero-shot video editing," *CoRR*, vol. abs/2312.10656, 2023. [7](#), [8](#), [15](#), [17](#)
- [168] T. Miyato, T. Kataoka, M. Koyama, and Y. Yoshida, "Spectral normalization for generative adversarial networks," in *ICLR*, 2018. [7](#), [18](#)
- [169] D. Hendrycks and K. Gimpel, "Gaussian error linear units (gelus)," *CoRR*, vol. abs/1606.08415, 2016. [7](#)
- [170] J. Lin, C. Gan, and S. Han, "TSM: temporal shift module for efficient video understanding," in *ICCV*. IEEE, 2019, pp. 7082–7092. [8](#)
- [171] R. Ranftl, K. Lasinger, D. Hafner, K. Schindler, and V. Koltun, "Towards robust monocular depth estimation: Mixing datasets for zero-shot cross-dataset transfer," *IEEE Trans. Pattern Anal. Mach. Intell.*, vol. 44, no. 3, pp. 1623–1637, 2022. [8](#), [18](#)
- [172] L. H. Li, P. Zhang, H. Zhang, J. Yang, C. Li, Y. Zhong, L. Wang, L. Yuan, L. Zhang, J. Hwang, K. Chang, and J. Gao, "Grounded language-image pre-training," in *CVPR*. IEEE, 2022, pp. 10955–10965. [8](#)
- [173] S. Ge, S. Nah, G. Liu, T. Poon, A. Tao, B. Catanzaro, D. Jacobs, J. Huang, M. Liu, and Y. Balaji, "Preserve your own correlation: A noise prior for video diffusion models," in *ICCV*. IEEE, 2023, pp. 22873–22884. [8](#), [11](#)
- [174] Z. Su, W. Liu, Z. Yu, D. Hu, Q. Liao, Q. Tian, M. Pietikäinen, and L. Liu, "Pixel difference networks for efficient edge detection," in *ICCV*. IEEE, 2021, pp. 5097–5107. [8](#)
- [175] J. Li, D. Li, C. Xiong, and S. C. H. Hoi, "BLIP: bootstrapping language-image pre-training for unified vision-language understanding and generation," in *ICML*, vol. 162. PMLR, 2022, pp. 12888–12900. [9](#)
- [176] OpenAI, "ChatGPT," <https://openai.com/chatgpt/>, 2022. [9](#)
- [177] M. Bain, A. Nagrani, G. Varol, and A. Zisserman, "Frozen in time: A joint video and image encoder for end-to-end retrieval," in *ICCV*. IEEE, 2021, pp. 1708–1718. [9](#)
- [178] T. Ren, S. Liu, A. Zeng, J. Lin, K. Li, H. Cao, J. Chen, X. Huang, Y. Chen, F. Yan, Z. Zeng, H. Zhang, F. Li, J. Yang, H. Li, Q. Jiang, and L. Zhang, "Grounded SAM: assembling open-world models for diverse visual tasks," *CoRR*, vol. abs/2401.14159, 2024. [10](#)
- [179] H. K. Cheng and A. G. Schwing, "Xmem: Long-term video object segmentation with an atkinson-shiffrin memory model," in *ECCV*, vol. 13688. Springer, 2022, pp. 640–658. [10](#)
- [180] L. A. Gatys, A. S. Ecker, and M. Bethge, "A neural algorithm of artistic style," *CoRR*, vol. abs/1508.06576, 2015. [10](#)
- [181] Q. Wang, X. Bai, H. Wang, Z. Qin, and A. Chen, "Instantid: Zero-shot identity-preserving generation in seconds," *CoRR*, vol. abs/2401.07519, 2024. [10](#)
- [182] X. Chen, L. Huang, Y. Liu, Y. Shen, D. Zhao, and H. Zhao, "Anydoor: Zero-shot object-level image customization," *CoRR*, vol. abs/2307.09481, 2023. [10](#)
- [183] W. Lai, J. Huang, O. Wang, E. Shechtman, E. Yumer, and M. Yang, "Learning blind video temporal consistency," in *ECCV*, vol. 11219. Springer, 2018, pp. 179–195. [10](#)
- [184] D. Watson, J. Ho, M. Norouzi, and W. Chan, "Learning to efficiently sample from diffusion probabilistic models," *CoRR*, vol. abs/2106.03802, 2021. [11](#)
- [185] D. Watson, W. Chan, J. Ho, and M. Norouzi, "Learning fast samplers for diffusion models by differentiating through sample quality," in *ICLR*, 2022. [11](#)
- [186] W. Wang, Q. Lai, H. Fu, J. Shen, H. Ling, and R. Yang, "Salient object detection in the deep learning era: An in-depth survey," *IEEE Trans. Pattern Anal. Mach. Intell.*, vol. 44, no. 6, pp. 3239–3259, 2022. [11](#)
- [187] Y. Cheng, L. Li, Y. Xu, X. Li, Z. Yang, W. Wang, and Y. Yang, "Segment and track anything," *CoRR*, vol. abs/2305.06558, 2023. [12](#)
- [188] B. Cheng, I. Misra, A. G. Schwing, A. Kirillov, and R. Girdhar, "Masked-attention mask transformer for universal image segmentation," in *CVPR*. IEEE, 2022, pp. 1280–1289. [12](#)
- [189] S. Xie and Z. Tu, "Holistically-nested edge detection," in *ICCV*. IEEE Computer Society, 2015, pp. 1395–1403. [12](#)
- [190] P. Truong, M. Danelljan, F. Yu, and L. V. Gool, "Probabilistic warp consistency for weakly-supervised semantic correspondences," in *CVPR*. IEEE, 2022, pp. 8698–8708. [13](#)
- [191] X. Pan, A. Tewari, T. Leimkühler, L. Liu, A. Meka, and C. Theobalt, "Drag your GAN: interactive point-based manipulation on the generative image manifold," in *SIGGRAPH*. ACM, 2023, pp. 78:1–78:11. [13](#)
- [192] T. Karras, S. Laine, M. Aittala, J. Hellsten, J. Lehtinen, and T. Aila, "Analyzing and improving the image quality of stylegan," in *CVPR*. IEEE, 2020, pp. 8107–8116. [13](#)
- [193] Y. Shi, C. Xue, J. Pan, W. Zhang, V. Y. F. Tan, and S. Bai, "Dragdiffusion: Harnessing diffusion models for interactive point-based image editing," *CoRR*, vol. abs/2306.14435, 2023. [13](#)

- [194] C. Mou, X. Wang, J. Song, Y. Shan, and J. Zhang, "Dragondiffusion: Enabling drag-style manipulation on diffusion models," *CoRR*, vol. abs/2307.02421, 2023. [13](#)
- [195] P. Ling, L. Chen, P. Zhang, H. Chen, Y. Jin, and J. Zheng, "Free-drag: Feature dragging for reliable point-based image editing," in *CVPR*. IEEE, 2024, pp. 6860–6870. [13](#)
- [196] W. Bian, Z. Huang, X. Shi, Y. Dong, Y. Li, and H. Li, "Context-pips: Persistent independent particles demands spatial context features," *CoRR*, vol. abs/2306.02000, 2023. [13](#)
- [197] J. Yang, M. Gao, Z. Li, S. Gao, F. Wang, and F. Zheng, "Track anything: Segment anything meets videos," *CoRR*, vol. abs/2304.11968, 2023. [13](#)
- [198] A. Radford, J. W. Kim, C. Hallacy, A. Ramesh, G. Goh, S. Agarwal, G. Sastry, A. Askell, P. Mishkin, J. Clark, G. Krueger, and I. Sutskever, "Learning transferable visual models from natural language supervision," in *ICML*, vol. 139. PMLR, 2021, pp. 8748–8763. [14](#), [16](#)
- [199] J. Fu, S. Li, Y. Jiang, K. Lin, C. Qian, C. C. Loy, W. Wu, and Z. Liu, "Stylegan-human: A data-centric odyssey of human generation," in *ECCV*, vol. 13676. Springer, 2022, pp. 1–19. [14](#)
- [200] Y. Ge, R. Zhang, X. Wang, X. Tang, and P. Luo, "Deepfashion2: A versatile benchmark for detection, pose estimation, segmentation and re-identification of clothing images," in *CVPR*. IEEE, 2019, pp. 5337–5345. [14](#)
- [201] Y. Jafarian and H. S. Park, "Learning high fidelity depths of dressed humans by watching social media dance videos," in *CVPR*. IEEE, 2021, pp. 12753–12762. [14](#)
- [202] T. Lin, M. Maire, S. J. Belongie, J. Hays, P. Perona, D. Ramanan, P. Dollár, and C. L. Zitnick, "Microsoft COCO: common objects in context," in *ECCV*, vol. 8693. Springer, 2014, pp. 740–755. [14](#)
- [203] J. Z. Wu, X. Li, D. Gao, Z. Dong, J. Bai, A. Singh, X. Xiang, Y. Li, Z. Huang, Y. Sun, R. He, F. Hu, J. Hu, H. Huang, H. Zhu, X. Cheng, J. Tang, M. Z. Shou, K. Keutzer, and F. N. Iandola, "CVPR 2023 text guided video editing competition," *CoRR*, vol. abs/2310.16003, 2023. [14](#)
- [204] A. Blattmann, T. Dockhorn, S. Kulal, D. Mendelevitch, M. Kilian, D. Lorenz, Y. Levi, Z. English, V. Voleti, A. Letts, V. Jampani, and R. Rombach, "Stable video diffusion: Scaling latent video diffusion models to large datasets," *CoRR*, vol. abs/2311.15127, 2023. [15](#), [18](#)
- [205] J. Yu, Z. Wang, V. Vasudevan, L. Yeung, M. Seyedhosseini, and Y. Wu, "Coca: Contrastive captioners are image-text foundation models," *Trans. Mach. Learn. Res.*, vol. 2022, 2022. [15](#)
- [206] K. P. Yu, Z. Zhang, F. Hu, and J. Chai, "Efficient in-context learning in vision-language models for egocentric videos," *CoRR*, vol. abs/2311.17041, 2023. [15](#)
- [207] OpenAI, "GPT-4o," <https://openai.com/index/hello-gpt-4o/>, 2024. [15](#)
- [208] C. Schuhmann, R. Vencu, R. Beaumont, R. Kaczmarczyk, C. Mullis, A. Katta, T. Coombes, J. Jitsev, and A. Komatsuzaki, "LAION-400M: open dataset of clip-filtered 400 million image-text pairs," *CoRR*, vol. abs/2111.02114, 2021. [16](#)
- [209] H. Wu, E. Zhang, L. Liao, C. Chen, J. Hou, A. Wang, W. Sun, Q. Yan, and W. Lin, "Exploring video quality assessment on user generated contents from aesthetic and technical perspectives," in *ICCV*. IEEE, 2023, pp. 20087–20097. [16](#)
- [210] M. Caron, H. Touvron, I. Misra, H. Jégou, J. Mairal, P. Bojanowski, and A. Joulin, "Emerging properties in self-supervised vision transformers," in *ICCV*. IEEE, 2021, pp. 9630–9640. [16](#)
- [211] M. Oquab, T. Darcet, T. Moutakanni, H. Vo, M. Szafraniec, V. Khalidov, P. Fernandez, D. Haziza, F. Massa, A. El-Nouby, M. Assran, N. Ballas, W. Galuba, R. Howes, P. Huang, S. Li, I. Misra, M. G. Rabbat, V. Sharma, G. Synnaeve, H. Xu, H. Jégou, J. Mairal, P. Labatut, A. Joulin, and P. Bojanowski, "Dinov2: Learning robust visual features without supervision," *CoRR*, vol. abs/2304.07193, 2023. [16](#)
- [212] Y. Wang, Y. He, Y. Li, K. Li, J. Yu, X. Ma, X. Chen, Y. Wang, P. Luo, Z. Liu, Y. Wang, L. Wang, and Y. Qiao, "Internvid: A large-scale video-text dataset for multimodal understanding and generation," *CoRR*, vol. abs/2307.06942, 2023. [16](#), [18](#)
- [213] Y. Kirstain, A. Polyak, U. Singer, S. Matiana, J. Penna, and O. Levy, "Pick-a-pic: An open dataset of user preferences for text-to-image generation," in *NeurIPS*, 2023. [16](#)
- [214] H. Xue, T. Hang, Y. Zeng, Y. Sun, B. Liu, H. Yang, J. Fu, and B. Guo, "Advancing high-resolution video-language representation with large-scale video transcriptions," in *CVPR*. IEEE, 2022, pp. 5026–5035. [18](#)
- [215] W. Wang and Y. Yang, "Vidprom: A million-scale real prompt-gallery dataset for text-to-video diffusion models," *CoRR*, vol. abs/2403.06098, 2024. [18](#)
- [216] T. Chen, A. Siarohin, W. Menapace, E. Deyneka, H. Chao, B. E. Jeon, Y. Fang, H. Lee, J. Ren, M. Yang, and S. Tulyakov, "Panda-70m: Captioning 70m videos with multiple cross-modality teachers," *CoRR*, vol. abs/2402.19479, 2024. [18](#)
- [217] A. Sauer, D. Lorenz, A. Blattmann, and R. Rombach, "Adversarial diffusion distillation," *CoRR*, vol. abs/2311.17042, 2023. [18](#)
- [218] Y. Song, P. Dhariwal, M. Chen, and I. Sutskever, "Consistency models," in *ICML*, vol. 202. PMLR, 2023, pp. 32211–32252. [18](#)
- [219] C. Meng, R. Rombach, R. Gao, D. P. Kingma, S. Ermon, J. Ho, and T. Salimans, "On distillation of guided diffusion models," in *CVPR*. IEEE, 2023, pp. 14297–14306. [18](#)
- [220] T. Yin, M. Gharbi, R. Zhang, E. Shechtman, F. Durand, W. T. Freeman, and T. Park, "One-step diffusion with distribution matching distillation," *CoRR*, vol. abs/2311.18828, 2023. [18](#)
- [221] S. Luo, Y. Tan, L. Huang, J. Li, and H. Zhao, "Latent consistency models: Synthesizing high-resolution images with few-step inference," *CoRR*, vol. abs/2310.04378, 2023. [18](#)
- [222] C. Xu, T. Song, W. Feng, X. Li, T. Ge, B. Zheng, and L. Wang, "Accelerating image generation with sub-path linear approximation model," *CoRR*, vol. abs/2404.13903, 2024. [18](#)
- [223] W. Peebles and S. Xie, "Scalable diffusion models with transformers," in *ICCV*. IEEE, 2023, pp. 4172–4182. [18](#)
- [224] B. Lefaudeux, F. Massa, D. Liskovich, W. Xiong, V. Caggiano, S. Naren, M. Xu, J. Hu, M. Tintore, S. Zhang, P. Labatut, D. Haziza, L. Wehrstedt, J. Reizenstein, and G. Sizov, "xFormers: A modular and hackable transformer modelling library," <https://github.com/facebookresearch/xformers>, 2022. [18](#)